Acta Physiologica

RESEARCH PAPER

Succinate Modulation as a Biochemical Correlate of Metabolic and Neurobehavioral Changes Associated With Intermittent Fasting in Obesity

Andrea Tognozzi[1,2] | Fabrizia Carli[3] | Sherif Abdelkarim[4] | Sara Cornuti[2] | Francesca Damiani[2] | Maria Grazia Giuliano[5] | Alice Miniati[5] | Martina Nasisi[3] | Lia De Benedictis[3] | Kousha Changizi Ashtiani[4] | Gaia Scabia[3] | Margherita Maffei[3] | Pierre Baldi[4] | Amalia Gastaldelli[3,5] | Paola Tognini[5]

[1]Department of Translational Research and New Technologies in Medicine and Surgery, University of Pisa, Pisa, Italy | [2]Laboratory of Biology, Scuola Normale Superiore, Pisa, Italy | [3]Institute of Clinical Physiology, National Research Council, Pisa, Italy | [4]AI in Science Institute, School of Information and Computer Sciences, University of California, Irvine, Irvine, California, USA | [5]Health Science Interdisciplinary Center, Scuola Superiore Sant'Anna, Pisa, Italy

Correspondence: Amalia Gastaldelli (amalia.gastaldelli@cnr.it) | Paola Tognini (paola.tognini@santannapisa.it)

Received: 10 September 2025 | **Revised:** 20 November 2025 | **Accepted:** 29 November 2025

Keywords: behavior | high fat diet | hippocampus | intermittent fasting | neuroinflammation | obesity | succinate

ABSTRACT

Aim: Obesity significantly impacts the central nervous system (CNS), increasing the risks of neuropsychiatric disorders and dementia. Intermittent fasting (IF) shows promise for improving peripheral and CNS health, but its mechanisms are unclear.

Methods: Using a diet-induced obesity mouse model [10 weeks high fat diet (HFD), then 4 weeks intervention], we compared HFD, HFD-IF, ad libitum control chow (CC), and CC-IF groups.

Results: Switching to CC or IF reduced body weight, fat mass, and improved glucose tolerance. Notably, CC-IF uniquely enhanced exploration and reduced anxiety-like behavior. Transcriptomics revealed HFD-induced hippocampal neuroinflammation, whereas metabolomics identified a specific succinate signature in CC-IF mice: plasma concentration decreased, whereas liver and brown adipose tissue (BAT) levels increased. Succinate supplementation mimicked CC-IF metabolic and behavioral benefits and reduced hippocampal inflammation.

Conclusion: These findings suggest that regulating plasma succinate and its metabolism in liver and BAT may represent a novel biochemical correlate underlying the metabolic, neuroinflammatory, and behavioral improvements induced by IF.

1 | Introduction

Excessive body weight and obesity are well-established risk factors for the development of numerous comorbidities, including hypertension, type 2 diabetes, stroke, ischemic heart disease, and certain types of cancer [1–3]. Obesity is also linked to cognitive decline and an increased risk for neurological disorders such as dementia and Alzheimer's disease (AD) [4–8]. Notably, post-mortem studies of individuals with severe obesity frequently hallmark pathological features of AD, including β-amyloid deposits and β-amyloid precursor proteins [9]. Furthermore, high body mass index (BMI) has been correlated with deficits in learning, memory, attention, and decision-making [10–14]. These cognitive impairments

Lead Contact: Requests for further information, resources, and reagents should be directed to and will be fulfilled by the lead contact, Paola Tognini (paola.tognini@santannapisa.it).

are often associated with structural and volumetric changes in the brain, particularly in regions vital for memory and executive function, such as the hippocampus and prefrontal cortex [15–18].

Preclinical studies consistently demonstrate that western diets, characterized by high-fat and high-sugar intake, as well as high-fat diets (HFD), are associated with a spectrum of cognitive deficits, including impaired learning, memory, increased anxiety- and depression-like behaviors [19–25]. These effects highlight the detrimental impact of diet-induced obesity (DIO) on brain health, further underscoring the urgent need for effective interventions.

Although traditional low-calorie balanced diets have long been recognized for their benefits in weight loss and metabolic improvements, recent research suggests that intermittent fasting (IF) may offer distinct and, in some cases, superior advantages. IF, which alternates periods of restricted caloric intake with unrestricted eating, has been shown to improve insulin sensitivity, regulate blood glucose levels, and positively affect lipid profiles in both humans and animal models [26–33]. In addition to its metabolic benefits, fasting extends lifespan [33, 34], and exerts powerful neuroprotective effects, enhancing cognitive performance, reducing anxiety, and offering protection against depression [35–40]. Fasting has been found to modulate the transcriptional and epigenetic landscape of the brain, particularly within the cerebral cortex [41], suggesting profound, system-wide effects beyond mere metabolic improvements.

Despite the recognized benefits of both dietary approaches, the comparative impact of IF versus low-calorie diets on brain function in the context of obesity remains incompletely understood. IF may activate distinct or complementary molecular pathways that further enhance brain health in a condition of metabolic dysfunction.

In the current study, we aimed to explore how IF and ad libitum consumption of a balanced control chow (CC) diet influence metabolic parameters, cognitive function, and behaviors in a DIO mouse model. Male mice were initially fed an HFD for 10 weeks, followed by random allocation into four experimental groups for an additional 4 weeks: a group continuing on the HFD (HFD group), a group subjected to IF by receiving the HFD every other day (HFD-IF), a group fed a balanced control chow diet ad libitum (CC), and a group subjected to IF with the CC every other day (CC-IF).

Metabolic and behavioral correlates were investigated, revealing that CC-IF was particularly effective in reducing body weight (BW) and improving anxiety-like behavior.

To further elucidate the molecular mechanisms underlying the metabolic and brain-related effects of IF, we conducted a transcriptomic experiment on liver and hippocampal tissues. Gene ontology (GO) analysis revealed that inflammatory and immune-related pathways were prominently dysregulated in the hippocampus of HFD mice. Additionally, metabolomic profiling identified a significant increase in succinate levels in the liver and brown adipose tissue (BAT), but a decrease in plasma, specific to CC-IF. To investigate the association between succinate changes and CC-IF, we administered sodium succinate to DIO mice and explored its effects on BW reduction, behavior modulation, and hippocampal inflammation.

2 | Results

2.1 | Metabolic Effects of Dietary Switch to Intermittent Fasting or an Ad Libitum Balanced Diet After 10-Week HFD Feeding

To investigate and compare how dietary interventions, such as IF or a balanced low-calorie diet, affect metabolism in DIO mice, male C57BL/6J mice were fed a HFD for 10 weeks. From week 11 to week 14, mice were subjected to a diet switch (Figure 1a). BW was measured weekly, and as anticipated, HFD feeding led to a continuous increase in BW from week 1 (Figure 1b). Transitioning to the HFD-IF, CC, and CC-IF regimens resulted in a significant BW reduction compared to the HFD group (Figure 1b). Notably, both the CC and CC-IF interventions induced greater weight loss compared to HFD-IF, with the CC-IF group showing a more pronounced reduction during weeks 12 and 13 compared to the CC group (Figure 1b, see Table S1 for the complete statistics).

During the 14th week, fasting blood glucose levels were measured across all experimental groups. The transition to CC and CC-IF diets resulted in a significant reduction in glycemia compared to HFD-fed mice (Figure 1c). In contrast, 4 weeks of HFD-IF did not induce a significant decrease in fasting blood glucose (Figure 1c). To further assess glucose metabolism, we conducted an oral glucose tolerance test (OGTT). After 14 weeks of HFD feeding, mice exhibited glucose intolerance, characterized by elevated blood glucose levels at time 0 and a failure to return to baseline within 2 h post-glucose administration (Figure 1d). Notably, the HFD-IF, CC, and CC-IF regimens all effectively restored glucose tolerance following DIO, with no significant differences observed among the three dietary interventions (Figure 1d, see Table S1 for full statistical analysis). Consistent with these findings, HFD-fed mice showed elevated plasma insulin levels, which decreased upon dietary switch and reached significance in CC-IF conditions (Figure 1e). This suggests that HFD-induced hyperglycemia may be attributed to a loss of insulin sensitivity and subsequent impairment in glucose uptake by specific tissues, potentially driven by increased lipid metabolism [42, 43]. Furthermore, plasma leptin levels were significantly elevated in HFD-fed mice compared to the other three groups (Figure 1f), because of increased fat depot accumulation [44]. Specifically, HFD mice exhibited a marked increase in white adipose tissue (WAT) depots, including perirenal, epididymal, and subcutaneous fat, compared to HFD-IF, CC, and CC-IF groups (Figure 1g–i). Notably, the CC-IF intervention was the most effective in reducing WAT, leading to a significant decrease in both epididymal and perirenal fat relative to the HFD-IF group (Figure 1g,h). These findings were consistent when evaluating total WAT weight, as well as when normalizing fat depot weights to individual BW (Figure S1). Additionally, interscapular brown adipose tissue (BAT) was significantly reduced to a similar extent across HFD-IF, CC, and CC-IF dietary interventions (Figures 1j and S1).

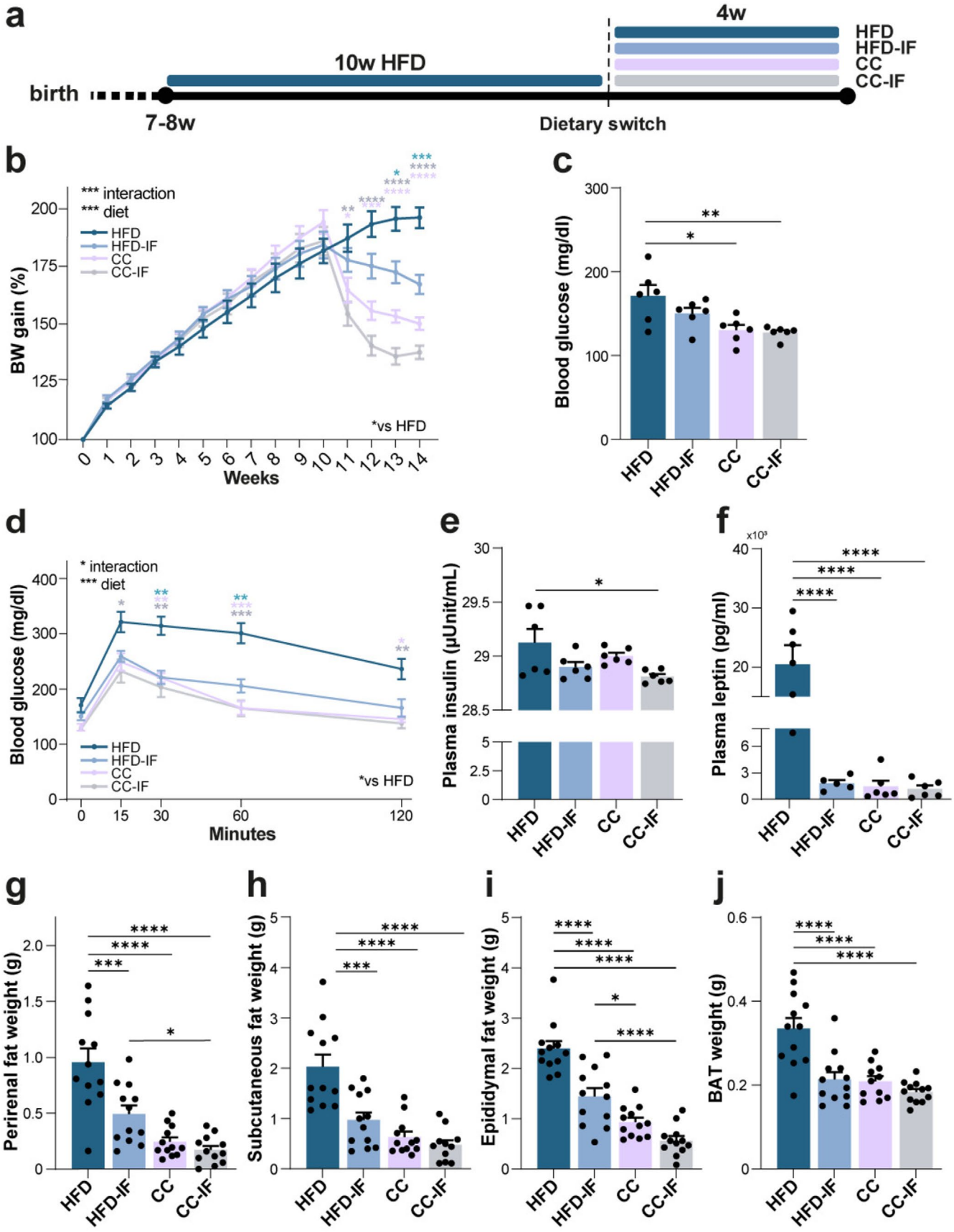

FIGURE 1 | Legend on next page.

FIGURE 1 | Changes in body weight and metabolic parameters driven by the dietary switch in DIO mice. (a) Experimental timeline. (b) Weekly measure of BW ($n=12$/group. Two-way RM ANOVA, diet × time interaction $p<0.0001$. See Table S1 for Tukey's post hoc comparisons). (c) Fasting glycemia ($n=6$/experimental group Two-way ANOVA, diet × feeding mode interaction $p=0.2971$, feeding mode $p=0.1604$, diet $p=0.001$. Tukey's post hoc, HFD vs. CC-IF $p=0.0062$, HFD vs. CC $p=0.0114$). (d) Oral glucose tolerance test ($n=6$/experimental group. Two-way RM ANOVA, diet × time interaction $p=0.0206$. See Table S1 for Tukey's post hoc comparisons). (e) Plasma insulin level ($n=6$/experimental group. Two-way ANOVA, diet × feeding mode interaction $p=0.7967$, feeding mode $p=0.0073$, diet $p=0.1438$. Tukey's post hoc, HFD vs. CC-IF $p=0.0221$). (f) Plasma leptin level ($n=5$ HFD-IF, $n=6$ HFD/CC/CC-IF. Two-way ANOVA, diet × feeding mode interaction $p<0.0001$, feeding mode $p<0.0001$, diet $p<0.0001$. Tukey's post hoc, HFD vs. CC-IF $p<0.0001$, HFD vs. CC $p<0.0001$, HFD vs. HFD-IF $p<0.0001$). (g) Perirenal fat weight ($n=12$/group. Two-way ANOVA, diet × feeding mode interaction $p=0.0135$, feeding mode $p=0.001$, diet $p<0.0001$. Tukey's post hoc, HFD vs. CC-IF $p<0.0001$, HFD vs. CC $p<0.0001$, HFD vs. HFD-IF $p=0.0005$, CC-IF vs. HFD-IF $p=0.0205$). (h) Subcutaneous fat weight ($n=12$/experimental group. Two-way ANOVA, diet × feeding mode interaction $p=0.0081$, feeding mode $p=0.0005$, diet $p<0.0001$. Tukey's post hoc, HFD vs. CC-IF $p<0.0001$, HFD vs. CC $p<0.0001$, HFD vs. HFD-IF $p=0.0002$). (i) Epididymal fat weight ($n=12$/group. Two-way ANOVA, diet × feeding mode interaction $p=0.0264$, feeding mode $p<0.0001$, diet $p<0.0001$. Tukey's post hoc, HFD vs. CC-IF $p<0.0001$, HFD vs. CC $p<0.0001$, HFD vs. HFD-IF $p<0.0001$, CC-IF vs. HFD-IF $p<0.0001$, CC vs. HFD-IF $p=0.0332$). (j) Brown adipose tissue weight ($n=12$/experimental group. Two-way ANOVA, diet × feeding mode interaction $p=0.0079$, feeding mode $p=0.0001$, diet $p<0.0001$. Tukey's post hoc, HFD vs. CC-IF $p<0.0001$, HFD vs. CC $p<0.0001$, HFD vs. HFD-IF $p<0.0001$). ANOVA factors: Diet = HFD vs. CC, feeding mode = ad libitum vs. IF. Error bars represent SEM. $^{*}p\leq0.05$, $^{**}p\leq0.01$ and $^{***}p\leq0.001$, $^{****}p\leq0.0001$.

All together these data demonstrate that switching to IF or ad libitum CC after 10 weeks HFD feeding had all significant effects on decreasing BW, fat depots, and improving glucose tolerance. However, CC-IF seems to be the dietary regimen with the strongest metabolic effects.

2.2 | CC-IF Ameliorates Exploratory and Anxiety-Like Behavior

Neuropsychiatric comorbidities, including anxiety, depression, mood disorders, and mild cognitive impairment, are frequent in obese individuals, with a subsequent reduction in the quality of life [45]. Behavioral abnormalities have also been described in rodent models of DIO.

Thus, to gain insights on the potential influence of switching to IF or an ad libitum balanced diet on behavioral performance in comparison to DIO mice, a battery of tests was performed during the last 10 days of feeding (Figure 2a).

First, we assessed anxiety-like behavior through the open-field (OF) test. No changes in velocity were observed among the groups (Figure S2a). Moreover, no significant alterations were found in the time spent in the center or in the corner of the arena (Figure 2b,c) or in the latency to enter the center (Figure 2d). Notably, although no differences were present in the total rearing or in the supported rearing (Figure S2b,c), both CC and CC-IF mice performed a higher number of unsupported rearing with respect to the HFD group (Figure 2e), indicating a willingness to explore the new environment and a potential decrease in anxiety [46].

Declarative memory performance was assessed using the Novel Object Recognition Test (NORT), which leverages the innate tendency of mice to spend more time exploring a novel object compared to a familiar one. After a 24-h retention interval (testing phase), no significant differences were observed in the preference index among the experimental groups, suggesting that the ability to recognize the familiar object remained intact across all the dietary conditions (Figure 2f).

The Y-maze test was performed to obtain an estimation of working memory and spontaneous exploratory behavior. The CC-IF group displayed a significant increase in the number of total entries, compared to HFD and HFD-IF, whereas a trend was identified comparing it to the CC treatment (Figure 2g). Furthermore, the number of alternate triads of the CC-IF showed the same results (Figure 2h), suggesting a higher exploratory behavior. On the other hand, no changes were found in the % of alternation parameters, indicating no overt alterations in working memory (Figure S2d).

To further assess exploratory and anxiety-like behaviors, mice were tested in the elevated plus maze (EPM). CC-IF mice exhibited a greater number of entries into the open arm compared to the HFD and HFD-IF groups (Figure 2i). A main effect of IF was found in the time spent in the open arm (Figure 2j) compared to the ad libitum groups. No significant changes were observed in the number of entries in the closed arm (Figure S2e), whereas the CC-IF group showed a trend toward reduced time spent in the closed arm (Figure S2f).

Finally, to provide an overall summary of the behavioral findings, an emotionality score was calculated as an index of anxiety-like behavior [47]. This score revealed a marked difference between the CC-IF and HFD and HFD-IF mice (Figure 2k), confirming that CC-IF is the dietary regimen with the stronger effect on anxiety and exploration in comparison to the DIO condition.

2.3 | Hippocampus Transcriptome Analysis Revealed HFD-Driven Activation of Immune Processes and Distinct Transcriptional Responses-Driven by the Dietary Switches

Complex behavior such as exploration and emotional features involves several brain areas, including cortical and subcortical regions. To dissect the mechanisms underlying diet effects on mouse behavioral performance, and on the basis of our results pointing toward an improvement in exploration and anxiety-like behavior in CC-IF, we focused on the hippocampus (Figure 3a). RNA-sequencing (seq) experiments of all four

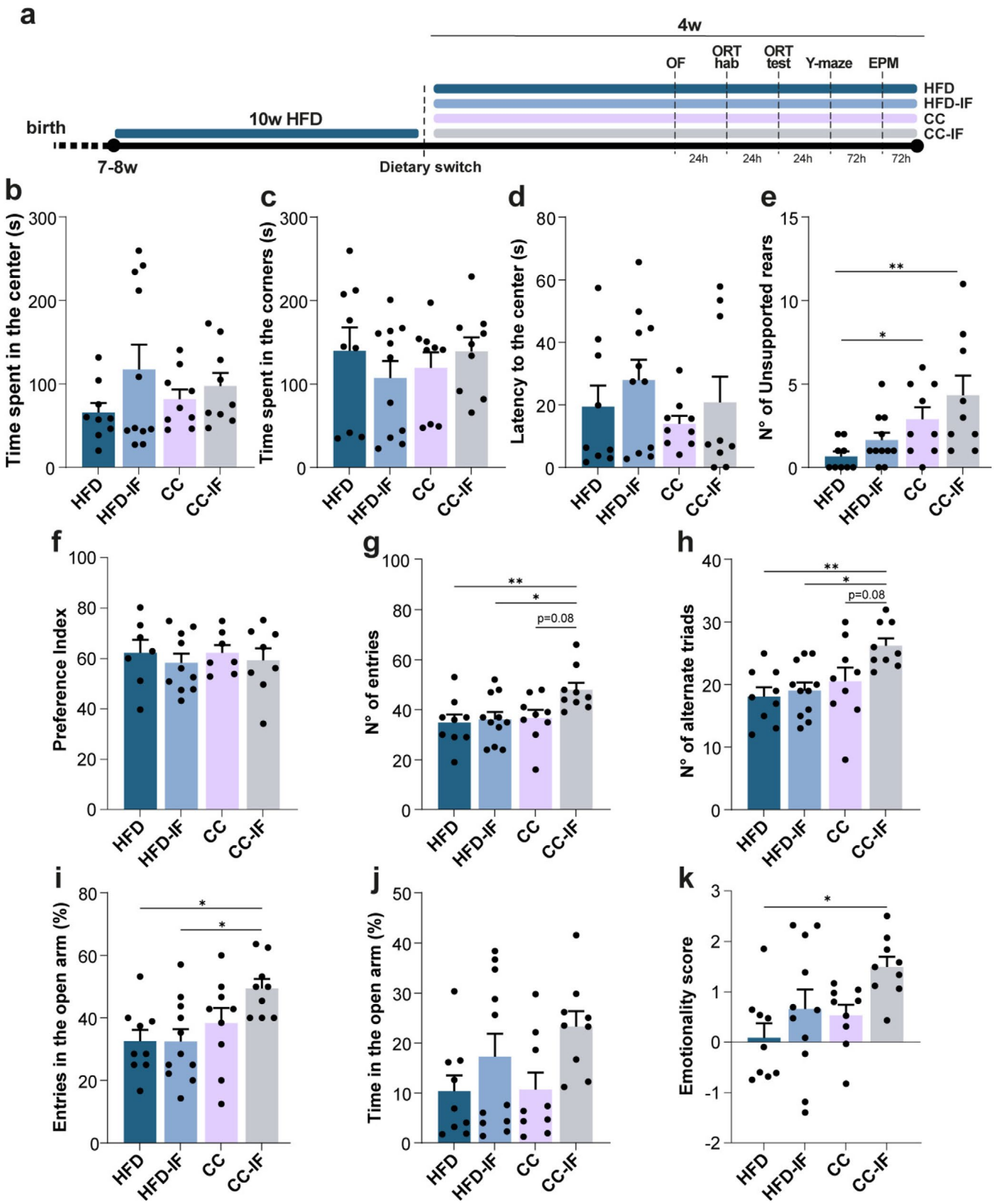

FIGURE 2 | Legend on next page.

experimental groups revealed significant gene expression differences in the three dietary switches with respect to HFD feeding (Table S2). GO analysis (Table S2) also highlighted distinct biochemical pathways. A total of 121 transcripts were differentially expressed in HFD vs. CC-IF conditions; specifically, 28 genes were downregulated, and 93 genes were upregulated in HFD (Figure S3a). Among the upregulated transcripts in HFD, the top annotations were related to immune system response and processes, antigen processing and presentation, aging (Figure S3b). The genes downregulated in HFD clustered in annotations

FIGURE 2 | Analysis of behavioral performance after the diet switch in DIO mice. (a) Experimental timeline. (b) Time spent in the center in the OF (Two-way ANOVA, diet × feeding mode interaction $p = 0.3807$, feeding mode $p = 0.1076$, diet $p = 0.922$). (c) Time spent in the corners in the OF (Two-way ANOVA, diet × feeding mode interaction $p = 0.2365$, feeding mode $p = 0.763$, diet $p = 0.791$). (d) Latency to enter in the central zone in the OF (Two-way ANOVA, diet × feeding mode interaction $p = 0.901$, feeding mode $p = 0.2396$, diet $p = 0.3348$). (e) Number of unsupported rears (Two-way ANOVA, diet × feeding mode interaction $p = 0.7431$, feeding mode $p = 0.1021$, diet $p = 0.0016$. Tukey's post hoc, HFD vs. CC-IF $p = 0.0064$, CC-IF vs. HFD-IF $p = 0.0478$). (f) NORT preference index (Two-way ANOVA, diet × feeding mode interaction $p = 0.3355$, feeding mode $p = 0.7412$, diet $p = 0.7647$). (g) Number of entries in the Y-maze test (Two-way ANOVA, diet × feeding mode, interaction $p = 0.1165$, feeding mode $p = 0.0494$, diet $p = 0.0328$. Tukey's post hoc, HFD vs. CC-IF $p = 0.0282$, CC-IF vs. HFD-IF $p = 0.0418$, CC vs. CC-IF $p = 0.0746$). (h) Y-maze number of alternate triads (Two-way ANOVA, diet × feeding mode, interaction $p = 0.1165$, feeding mode $p = 0.0494$, $p = 0.0328$. Tukey's post hoc, HFD vs. CC-IF $p = 0.0058$, CC-IF vs. HFD-IF $p = 0.012$, CC vs. CC-IF $p = 0.0794$). (i) Percentage of entries in the open arm in the EPM test (Two-way ANOVA, diet × feeding mode interaction $p = 0.1701$, feeding mode $p = 0.1758$, diet $p = 0.0077$. Tukey's post hoc, HFD vs. CC-IF $p = 0.0306$, CC-IF vs. HFD-IF $p = 0.0209$). (j) EPM percentage of time spent in the open arm (Two-way ANOVA, diet × feeding mode, interaction $p = 0.4621$, feeding mode $p = 0.0150$, diet $p = 0.405$). (k) Emotionality score. (Two-way ANOVA, diet × feeding mode interaction $p = 0.5341$, feeding mode $p = 0.017$, diet $p = 0.047$. Tukey's post hoc, HFD vs. CC-IF $p = 0.0167$). $N = 8$–11/experimental group. Error bars represent SEM. $^{*}p \leq 0.05$ and $^{**}p \leq 0.01$.

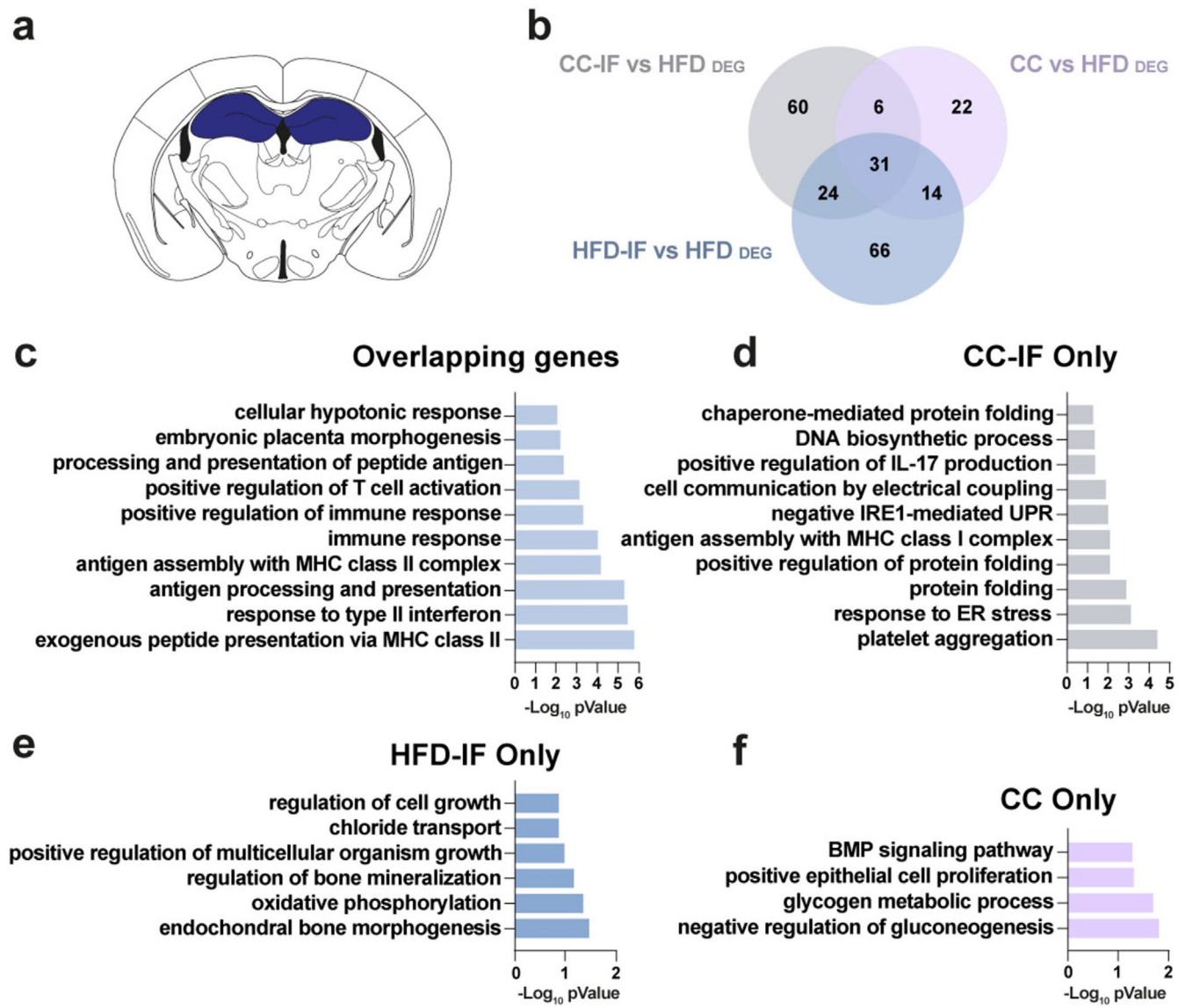

FIGURE 3 | Dietary regimen-dependent transcriptional changes in the hippocampus. (a) Schematic coronal section of the hippocampus showing the site of RNA-seq analysis. (b) Venn diagram illustrating the crossing of DEG (p-value < 0.1) between each of the 3 dietary interventions (HFD-IF, CC, CC-IF) compared to HFD. (c) GO biological processes analysis of 31 overlapping DEG. (d) GO biological processes analysis of 60 CC-IF exclusive DEG. (E) GO biological processes analysis of 66 HFD-IF exclusive DEG. (f) GO biological processes analysis of 22 CC exclusive DEG. $n = 4$ HFD/HFD-IF/CC, 3 CC-IF.

related to mRNA splicing and translation (Figure S3b). 73 transcripts were altered in the comparison HFD vs. CC (Figure S3a), with the 60 genes upregulated in the HFD group again clustering in pathways related to immune system response (Figure S3c). Finally, 135 transcripts were differentially expressed in the hippocampus of HFD vs. HFD-IF mice. Antigen processing, response to interferon gamma, and aging were again hits in the annotations of the 114 genes upregulated in HFD, whereas the transcripts upregulated in HFD-IF clustered in mRNA splicing and translation (Figure S3d). To have a better understanding of the common and specific pathways in CC-IF, CC, and HFD-IF with respect to HFD feeding, we crossed the differentially expressed transcripts of the three conditions in comparison with HFD. The Venn diagram demonstrated that 31 transcripts were commonly dysregulated in the three dietary regimens with respect to HFD (Figure 3b, and Table S3), and they clustered in annotations linked to immune system functions (Figure 3c and Table S3). The 60 differentially expressed genes specific to CC-IF clustered in biological pathways linked to protein folding, endoplasmic reticulum stress, and endosomal vesicle fusion (Figure 3d and Table S3). On the other hand, the 66 genes specific to HFD-IF response were grouped in annotations such as oxidative phosphorylation, chloride transport, and cell growth (Figure 3e and Table S3). CC-only genes clustered in pathways involved in metabolism, such as glycogen metabolic process and negative regulation of gluconeogenesis (Figure 3f and Table S3).

In summary, the transcriptome analysis revealed that HFD may drive immune response activation and potentially neuroinflammation in the hippocampus of mice. Furthermore, dietary switching to a low-calorie diet or IF after 10-week HFD causes hippocampus-specific transcriptional reprogramming.

2.4 | Liver Transcriptome and Metabolome Analysis Revealed Specific Alterations in TCA Cycle Metabolites

In parallel to hippocampal RNA-seq, we performed a liver transcriptome analysis (Table S4). Liver function is crucial to maintain metabolic homeostasis, and it is a key fasting-responsive organ, likely mediating many of the beneficial effects of IF [48, 49]. Indeed, hepatic tissue dramatically responded to diet changes. In the comparison of HFD vs. CC-IF, 768 genes were upregulated in HFD, whereas 769 transcripts were upregulated in CC-IF. In the comparison of HFD vs. CC, 274 genes were upregulated in HFD, and 189 were upregulated in CC. Finally, HFD liver displayed 281 genes upregulated with respect to HFD-IF, whereas 296 genes were downregulated (Figure S4a). Importantly, GO analysis (Table S4) showed that the transcripts increased by HFD feeding clustered in annotations such as lipid metabolic process, sterol biosynthetic process, steroid biosynthetic and metabolic process, cholesterol metabolic process, independent of the dietary switch (Figure S4b–d). We found common pathways related to circadian rhythms and circadian regulation of gene expression among the transcripts upregulated in the liver of CC-IF, CC, and HFD-IF fed mice (Figure S4b–d). As for the hippocampus, we crossed the differentially expressed transcripts of the 3 dietary switches (CC, CC-IF, and HFD-IF) in comparison with HFD (Figure 4a). The top annotation of the 81 common genes belonged to pathways linked to fatty acid and cholesterol metabolism. Response to glucose, circadian rhythms, and insulin secretion also came up in the analysis (Figure 4b and Table S5). The CC-IF vs. HFD comparison of 1066 specific transcripts displayed hits related to the regulation of transcription, translation, and chromatin organization (Figure 4c and Table S5). The 242 differentially expressed genes specific to the comparison of HFD vs. CC clustered in fatty acid and glutathione metabolic processes, response to stress (Figure 4d and Table S5). The 202 transcripts specific to the comparison of HFD-IF vs. HFD were related to extracellular matrix organization, cell migration, cell adhesion, and apoptosis (Figure 4e and Table S5).

Finally, we performed a metabolome analysis of liver, hippocampus, and plasma samples focusing on the TCA cycle metabolites and beta-hydroxy-butyrate (BHB). Not surprisingly, BHB was significantly increased in CC-IF and HFD-IF with respect to HFD and CC in the liver, plasma, and hippocampus (Figure 4f). Fumarate, malate, and alpha-keto-glutarate were significantly decreased in both CC-IF and HFD-IF liver in comparison to HFD (Figure 4g–i). Those results indicate an increase in TCA cycle activity in HFD liver, suggesting a potential increase in oxidative metabolism and subsequent oxidative stress [50]. Pyruvate and lactate displayed the same trend (Figure S4e), suggesting an effect of fasting on the enhancement of the gluconeogenic pathway independently of the type of food consumed. Moreover, CC-IF fumarate and malate were higher compared to CC (Figure 4g,h). Interestingly, succinate was the only metabolite among those analyzed to show an exclusive increase in the liver under the CC-IF condition (Figure 4j), and its levels were inversely correlated to BW (Figure S4f). This observation prompted us to extend the analysis of TCA cycle metabolites to plasma and brain tissues (Figure S4g,h). In plasma samples, malate and alpha-keto-glutarate were significantly increased in CC compared to HFD (Figure S4g). No differences were observed in pyruvate because of high variability, whereas plasma lactate reflected the liver situation (Figure S4g). In the hippocampus, fumarate, malate, and alpha-keto-glutarate displayed the same trend with an increase induced by the three dietary switches compared to HFD, although only malate reached statistical significance (Figure S4h). Pyruvate was unchanged, whereas lactate increased in CC with respect to CC-IF and HFD (Figure S4h). Hippocampal succinate was not altered (Figure S4h). Intriguingly, succinate levels in plasma were affected, showing a decrease in CC-IF (Figure 4k). Additionally, BAT succinate displayed a distinct increase in CC-IF mice (Figure 4l). These findings suggest a potential CC-IF-driven "sink effect" for circulating succinate, which may be utilized for thermogenesis in BAT [51], and possibly to provide the energy required for gluconeogenesis in the liver.

2.5 | Succinate Administration Improved Metabolic Parameters in DIO Mice

Succinate is a versatile molecule acting as a pivotal constituent in metabolic pathways and as a signaling metabolite in a paracrine and endocrine manner, influencing cell responses to a variety of stimuli [52]. Since the increase in liver and BAT succinate, and its decrease in plasma seemed to be a signature of weight loss and CC-IF, we decided to further explore the succinate's potential effects on mouse metabolism and behavioral

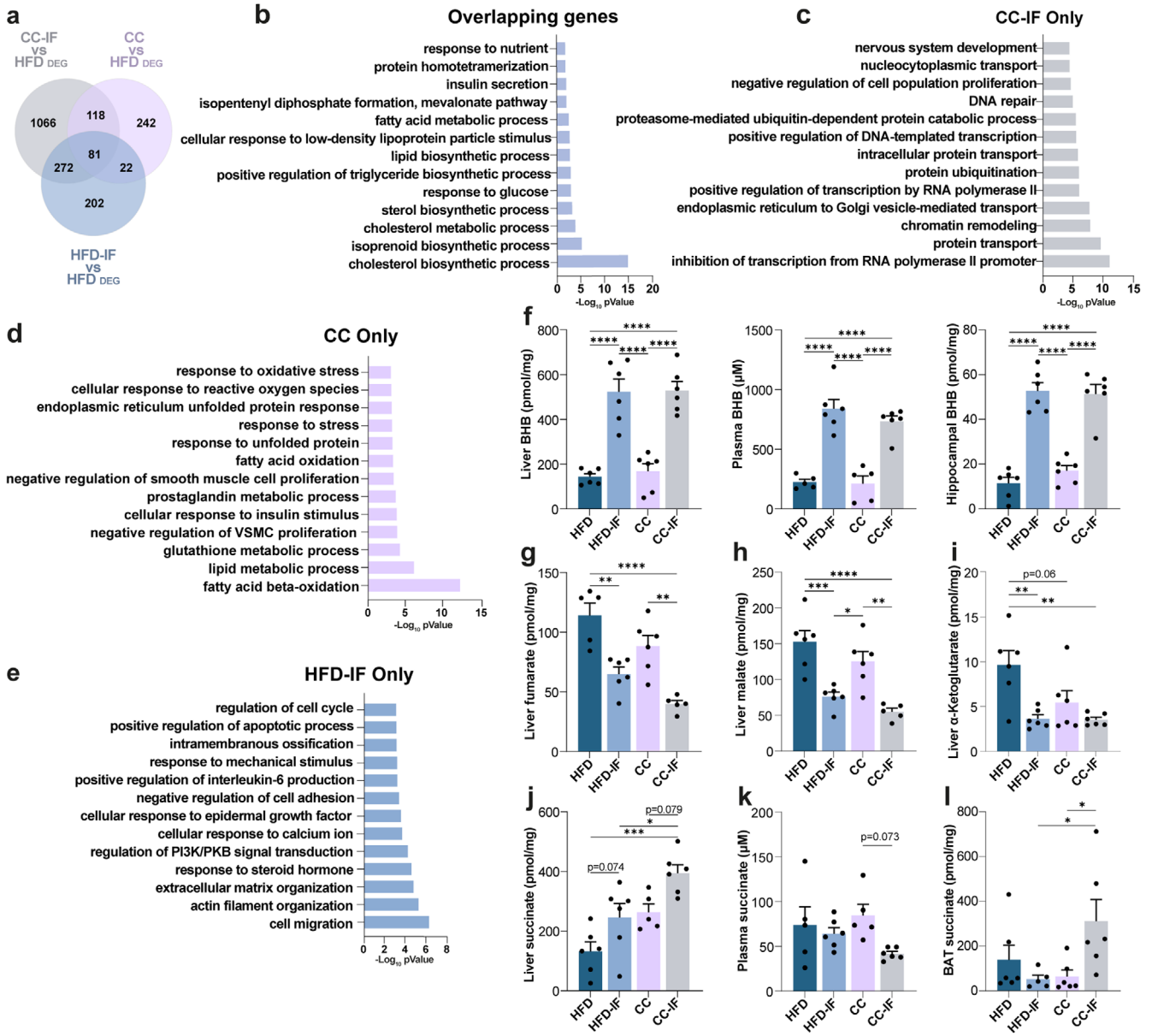

FIGURE 4 | Dietary regimen-dependent transcriptional changes in the liver and metabolomics analysis. (a) Venn diagram illustrating the crossing of DEG (p-value <0.05) between each of the 3 dietary interventions (HFD-IF, CC, CC-IF) in comparison with HFD. (b) GO biological processes analysis of 81 overlapping DEG. (c) GO biological processes analysis of 1066 CC-IF exclusive DEGs. (d) GO biological processes analysis of 242 CC exclusive DEG. (e) GO biological processes analysis of 202 HFD-IF exclusive DEG ($n=4$ HFD/CC/CC-IF, $n=2$ HFD-IF). (f) β-hydroxybutyrate concentration in liver, plasma and hippocampus. Liver: Two-way ANOVA, diet × feeding mode interaction $p=0.812$, feeding mode $p<0.0001$, diet $p=0.7016$. Tukey's post hoc, HFD vs. CC-IF $p<0.0001$, HFD, HFD vs. HFD-IF $p<0.0001$, CC vs. HFD-IF $p<0.0001$, CC vs. CC-IF $p<0.0001$; Plasma: Two-way ANOVA, diet × feeding mode interaction $p=0.4413$, feeding mode $p<0.0001$, diet $p=0.3307$. Tukey's post hoc, HFD vs. CC-IF $p<0.0001$, HFD vs. HFD-IF $p<0.0001$, CC vs. HFD-IF $p<0.0001$, CC vs. CC-IF $p<0.0001$; Hippocampus: Two-way ANOVA, diet × feeding mode interaction $p=0.3063$, feeding mode $p<0.0001$, diet $p=0.5214$. Tukey's post hoc, HFD vs. CC-IF $p<0.0001$, HFD vs. HFD-IF $p<0.0001$, CC vs. HFD-IF $p<0.0001$, CC vs. CC-IF $p<0.0001$. (g) Liver fumarate concentration (Two-way ANOVA, diet × treatment interaction $p=0.9755$, feeding mode $p<0.0001$, diet $p=0.004$. Tukey's post hoc, HFD vs. CC-IF $p<0.0001$, HFD vs. CC $p=0.1223$, HFD vs. HFD-IF $p=0.0014$, CC vs. CC-IF $p=0.0015$). (h) Liver Malate concentration (Two-way ANOVA, diet × feeding mode interaction $p=0.7982$, feeding mode $p<0.0001$, diet $p=0.0524$. Tukey's post hoc, HFD vs. CC-IF $p<0.0001$, HFD vs. HFD-IF $p=0.008$, CC vs. HFD-IF $p=0.0313$, CC vs. CC-IF $p=0.0028$). (i) Liver α-Ketoglutarate concentration (Two-way ANOVA, diet × feeding mode interaction $p=0.0741$, feeding mode $p=0.0018$, diet $p=0.0624$. Tukey's post hoc, HFD vs. CC-IF $p=0.0041$, HFD vs. CC $p=0.0578$, HFD vs. HFD-IF $p=0.0047$). (j) Liver Succinate concentration (Two-way ANOVA, diet × feeding mode interaction $p=0.8101$, feeding mode $p=0.0024$, diet $p=0.0008$. Tukey's post hoc, HFD vs. CC-IF $p=0.0002$, HFD vs. CC $p=0.0764$, CC-IF vs. HFD-IF $p=0.029$, CC vs. CC-IF $p=0.0788$). (k) Plasma succinate concentration (Two-way ANOVA, diet × feeding mode interaction $p=0.1638$, feeding mode $p=0.0357$, diet $p=0.6147$. Tukey's post hoc, CC vs. CC-IF $p=0.0731$). (l) BAT succinate concentration (Two-way ANOVA, diet × feeding mode interaction $p=0.017$, feeding mode $p=0.2255$, diet $p=0.1651$. Tukey's post hoc, CC-IF vs. HFD-IF $p=0.0507$, CC vs. CC-IF $p=0.0508$). Other comparisons were not significant. $N=5$–6/experimental group. Error bars represent SEM. *$p\leq0.05$, **$p\leq0.01$ and ***$p\leq0.001$, ****$p\leq0.0001$.

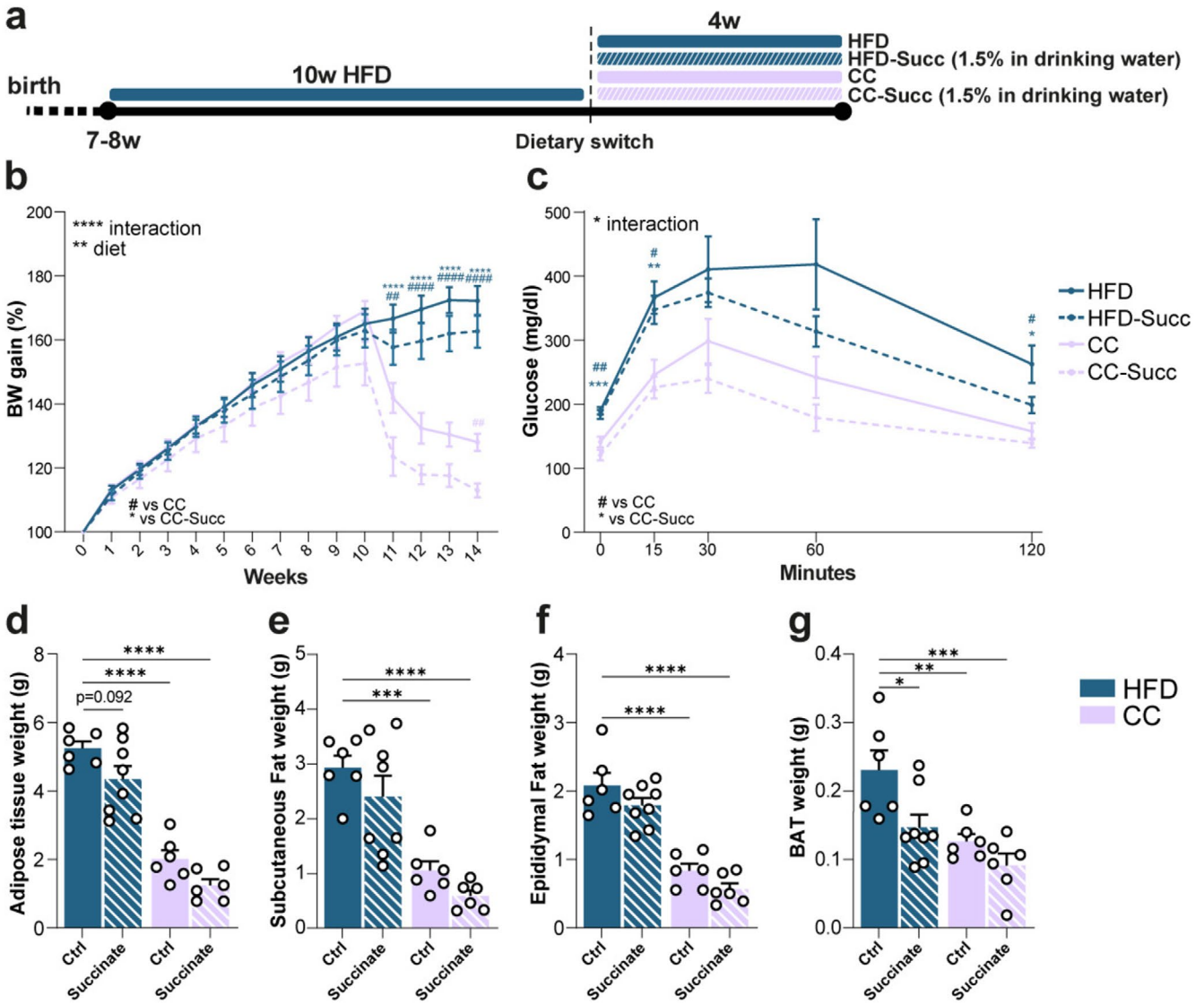

FIGURE 5 | Succinate administration affects body weight, glucose tolerance, and fat depots. (a) Experimental timeline. Mice were fed HFD for 10 weeks and then divided into four experimental groups for the following 4 weeks: One group continued on the HFD drinking regular water (HFD), another group was fed HFD drinking sodium succinate dissolved in water (HFD-Succ), a third group switched to CC drinking regular water (CC), and the fourth group was fed CC drinking sodium succinate (CC-Succ). (b) Weekly BW measure ($n = 11$ HFD, $n = 14$ HFD-Succ, $n = 11$ CC, $n = 12$ CC-Succ. Two-way RM ANOVA, diet × time interaction $p < 0.0001$. See Table S2 for Tukey's post hoc comparisons). (c) Oral glucose tolerance test (Two-way RM ANOVA, diet × time interaction $p = 0.0206$. See Table S2 for Dunnett's post hoc comparisons). (d) Total adipose tissue weight (Two-way ANOVA, diet × treatment interaction $p = 0.8379$, treatment $p = 0.01$, diet $p < 0.0001$. Dunnett's post hoc, HFD vs. HFD-Succ $p = 0.0921$, HFD vs. CC < 0.0001, HFD vs. CC-Succ $p < 0.0001$). (e) Subcutaneous fat weight (Two-way ANOVA, diet × treatment interaction $p = 0.9129$, treatment $p = 0.0822$, diet $p < 0.0001$. Dunnett's post hoc, HFD vs. HFD-Succ $p = 0.0921$, HFD vs. CC $p < 0.0001$, HFD vs. CC-Succ $p < 0.0001$). (f) Epididymal fat weight (Two-way ANOVA, diet × treatment interaction $p = 0.9573$, treatment $p = 0.039$, diet $p < 0.0001$. Dunnett's post hoc, HFD vs. HFD-Succ $p = 0.2573$, HFD vs. CC $p < 0.0001$, HFD vs. CC-Succ $p < 0.0001$). (g) BAT (Two-way ANOVA, diet × treatment interaction $p = 0.2416$, treatment $p = 0.039$, diet $p = 0.0007$. Dunnett's post hoc, HFD vs. HFD-Succ $p = 0.0156$, HFD vs. CC $p = 0.0051$, HFD vs. CC-Succ $p = 0.0003$). The label Control (Ctrl) under the graph bars refers to mice drinking regular water. ANOVA factors: Diet = HFD vs. CC, treatment = succinate vs. regular water. $N = 5$–8/experimental group, unless otherwise stated. Error bars represent SEM. *$p \leq 0.05$, **$p \leq 0.01$ and ***$p \leq 0.001$, ****$p \leq 0.0001$.

performance in our DIO model. To this end, after 10 weeks of HFD feeding, succinate dissolved in drinking water was administered to HFD and CC fed mice for the subsequent 4 weeks (Figure 5a). BW gain was monitored throughout the 14-week experiment. During the first 10 weeks of ad libitum HFD, all groups showed a steady increase in BW (Figure 5b). From week 11 to week 14, the HFD group continued to gain weight, whereas the CC group showed a marked reduction in BW. The CC-Succ group also displayed a significant BW decrease with respect to the previous HFD condition and in comparison to both HFD and HFD-Succ groups (Figure 5b). Notably, CC-Succ mice displayed a stronger drop in the BW with respect to CC, similarly to what we observed with the CC-IF intervention (Figure 1b), and the further decrease in BW was significant with respect to CC by week 14 (Figure 5b). Finally, the HFD-Succ group showed a slight reduction in BW compared to the HFD group, suggesting

that succinate supplementation may have an effect in mitigating the weight gain associated with an HFD (Figure 5b; for the complete statistics, see Table S6).

Glucose tolerance was impaired in HFD. Glycemia decreased 2 h post-glucose administration in HFD, although it remained significantly higher with respect to CC and CC-Succ (Figure 5c; for the complete statistics, see Table S6). In contrast, CC and CC-Succ had lower fasting blood glucose levels, and at 15 min post-glucose administration in comparison with the HFD groups (Figure 5c), indicating improved glucose tolerance. The HFD-Succ curve had a different trend in comparison to HFD. Indeed, glycemia started to decrease 30 min after glucose administration, a shared characteristic with the CC groups' curve, and went back to fasting levels after 120 min (Figure 5c). These data suggest that succinate supplementation could ameliorate glucose tolerance in HFD-fed mice. Importantly, the CC-Succ group consistently showed the most efficient glucose clearance throughout the test, returning to fasting levels by 60 min post-administration (Figure 5c).

Fat depot weight demonstrated the drastic effect of switching to CC. Indeed, total fat, subcutaneous fat, epididymal fat, and BAT were significantly decreased in both CC groups in comparison to HFD groups (Figure 5d–g and see Figure S5a for the analysis after normalization to the BW). Notably, there was a certain effect of succinate supplementation on total fat weight, showing a decrease (Figure 5d). Subcutaneous and epididymal fat displayed a slight trend toward a decrease (Figure 5e,f), whereas BAT was particularly influenced by succinate supplementation in the HFD comparison but not in the CC comparison (Figure 5g).

2.6 | Succinate Supplementation Improved Exploration and Anxiety-Like Behavior Similarly to CC-IF

To investigate the potential effect of succinate administration on brain function and evaluate similarities to the CC-IF regimen, mice were subjected to behavioral tests during the 14th week of diet (Figure 6a).

In the OF test, there was a HFD effect on velocity, demonstrating a reduction (Figure S5b). There were no significant changes in the time spent in the center, in the corner of the arena (Figure 6b,c) or in the latency to enter the center (Figure 6d). Supported rearing was increased by CC with respect to HFD, with no succinate influence (Figure 6e). When analyzing unsupported rearing behavior, we observed a notable effect of succinate supplementation that increased the number of rears in both CC and HFD-fed mice (Figure 6f). Finally, the total number of rears was increased in CC-Succ and CC compared to HFD, whereas a tendency to perform a higher number was present in HFD-Succ (Figure 6g). These data suggest that succinate may improve exploration and reduce overall anxiety-like behavior, regardless of the diet consumed by the animals.

In the Y-maze test, velocity reflected the previous observations from the OF test (Figure S5c). We observed a significant effect of the CC diet switch on the number of entries performed by the mice (Figure 6h). Succinate supplementation seemed to decrease the number of alternative triads performed by CC mice (Figure 6i); however, the percentage of alternation was affected neither by diet nor succinate (Figure 6j).

In the EPM, there were no differences in the four groups' velocity of exploration (Figure S5d). Neither diet nor succinate had effects on the number of entries into the open arm (Figure 6k). However, succinate supplementation to CC mice increased the time spent in the open arm compared to the HFD group (Figure 6l), suggesting a reduction in anxiety. Finally, CC-Succ displayed the higher emotionality score (Figure 6m), confirming the single behavioral test results. Overall, the behavioral data suggest that succinate may reduce anxiety-like behavior and improve exploration, particularly when transitioning to a CC diet.

2.7 | Succinate Supplementation Affects Inflammatory Marker Levels in the Hippocampus

Since the transcriptome analysis revealed that HFD may drive immune response activation and potentially neuroinflammation in the mouse hippocampus, we explored the expression of specific inflammatory markers. Hippocampal IL-1β expression analysis revealed a significant reduction with succinate supplementation, particularly when comparing CC to CC-Succ (Figure 7a). Similarly, TNFα expression was significantly lower in mice switched to a CC diet with succinate treatment, and a reduction trend was observed in HFD-Succ mice (Figure 7b).

On the basis of the above-mentioned results, we investigated microglia cells given their well-established role in neuroinflammation [53, 54] and since succinate seems to prevent their conversion to a pro-inflammatory state in vitro [55]. The density of microglial cells in the hippocampus was not affected by either diet or succinate treatment (Figure 7c). Microglial complexity, filament lengths, branching points, and terminal points were not significantly altered (Figure 7d–f). On the other hand, there was a main effect of diet on soma area and volume showing a decrease in CC compared to HFD (Figure 7g,h), whereas succinate showed a tendency to increase both measures (Figure 7g,h). Sphericity was not influenced by diet or succinate (Figure 7i).

All together, these data point toward a modulation of inflammation in the hippocampus by succinate administration, which may underscore the improved behavioral performance.

3 | Discussion

In this study, we investigated the metabolic and behavioral effects of three dietary interventions—CC, CC-IF, and HDF-IF—following DIO in mice. Our findings demonstrate that both CC and IF reversed the metabolic perturbations induced by chronic HFD consumption, albeit with distinct molecular and behavioral profiles. Indeed, CC-IF was exclusive in improving exploration and anxiety-like behavior. CC-IF was characterized by a decrease in plasma succinate and its potential shunt to the BAT and liver, which could influence energy expenditure and inflammatory responses. The IF regimen, consisting of every-other-day feeding in the mouse model, could raise some

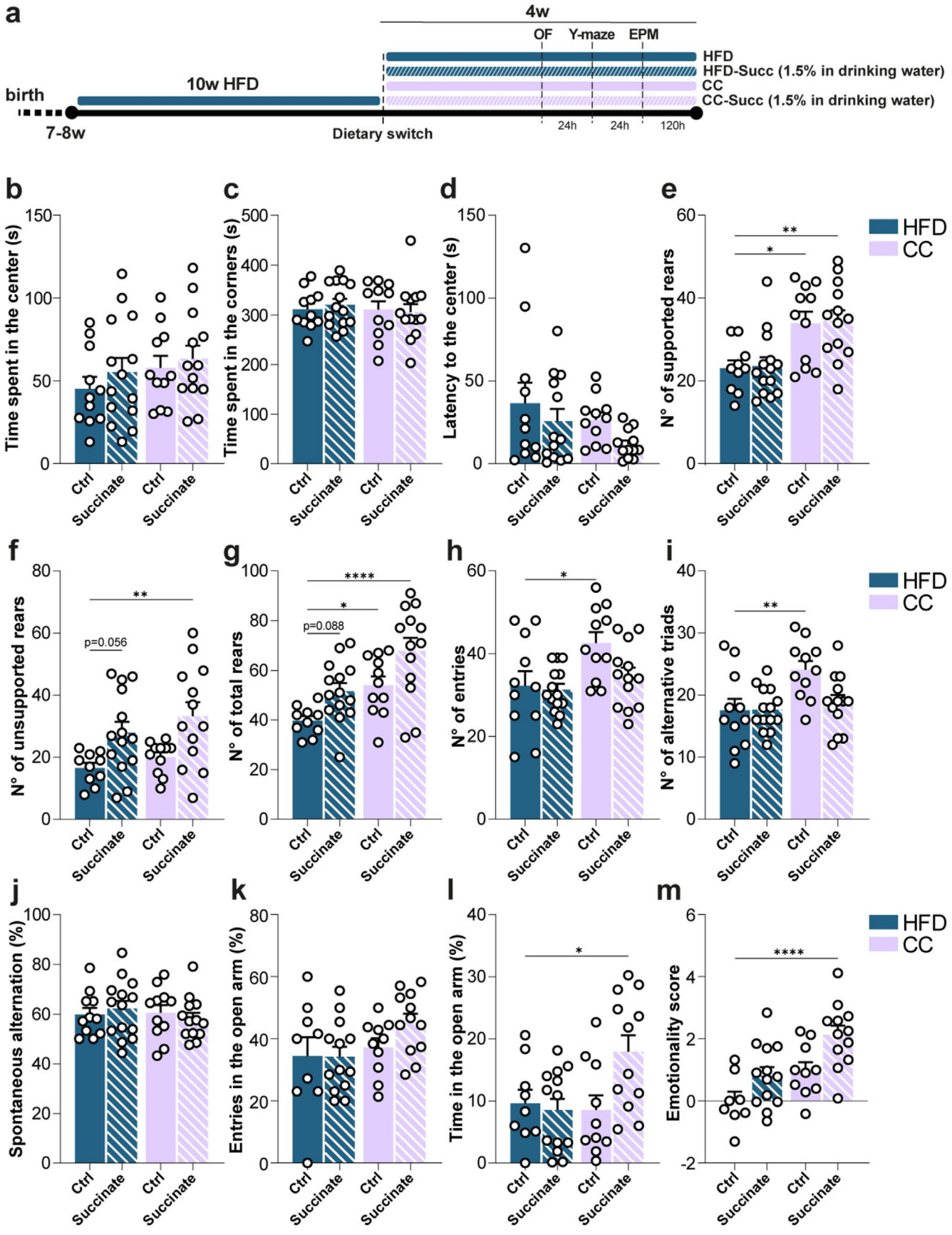

FIGURE 6 | Legend on next page.

FIGURE 6 | Succinate administration improves behavioral parameters. (a) Experimental timeline. (b) Time spent in the center of the OF (Two-way ANOVA, diet × treatment interaction $p = 0.7756$, treatment $p = 0.3318$, diet $p = 0.1994$). (c) Time spent in the corners in the OF (Two-way ANOVA, diet × treatment interaction $p = 0.6295$, treatment $p = 0.8741$, diet $p = 0.5938$). (d) Latency to enter the central zone in the OF (Two-way ANOVA, diet × treatment interaction $p = 0.7854$, treatment $p = 0.0947$, diet $p = 0.1161$). (e) Number of supported rears (Two-way ANOVA, diet × treatment interaction $p = 0.9858$, treatment $p = 0.8097$, diet $p < 0.0001$. Dunnett's post hoc, HFD vs. HFD-Succ $p = 0.9969$, HFD vs. CC $p = 0.0126$, HFD vs. CC-Succ $p = 0.0057$). (f) Number of unsupported rears (Two-way ANOVA, diet × treatment interaction $p = 0.7895$, treatment $p = 0.0007$, diet $p = 0.2002$. Dunnett's post hoc, HFD vs. HFD-Succ $p = 0.056$, HFD vs. CC $p = 0.8215$, HFD vs. CC-Succ $p = 0.0038$). (g) Number of total rears (Two-way ANOVA, diet × treatment interaction $p = 0.8076$, treatment $p = 0.0018$, diet $p = 0.0003$. Dunnett's post hoc, HFD vs. HFD-Succ $p = 0.0883$, HFD vs. CC $p = 0.0462$, HFD vs. HFD-Succ $p < 0.0001$). (h) Y-maze number of entries in the arms. (Two-way ANOVA, diet × treatment interaction $p = 0.1550$, treatment $p = 0.0704$, diet $p = 0.0078$. Dunnett's post hoc, HFD vs. HFD-Succ $p = 0.9825$, HFD vs. CC $p = 0.0176$, HFD vs. CC-Succ $p = 0.0176$). (i) Y-maze number of alternate triads (Two-way ANOVA, diet × treatment, interaction $p = 0.0514$, treatment $p = 0.06$, diet $p = 0.0069$. Dunnett's post hoc, HFD vs. HFD-Succ $p > 0.9999$, HFD vs. CC $p = 0.0059$, HFD vs. CC-Succ $p = 0.8568$). (j) Y-maze percentage of spontaneous alternation (Two-way ANOVA, diet × treatment interaction $p = 0.4118$, treatment $p = 0.9954$, diet $p = 0.5732$). (k) EPM percentage of entries in the open arm (Two-way ANOVA, diet × treatment, interaction $p = 0.2826$, treatment $p = 0.3106$, diet $p = 0.0764$). (l) EPM percentage of time spent in the open arm (Two-way ANOVA, diet × treatment interaction $p = 0.0293$, treatment $p = 0.0809$, diet $p = 0.0806$. Dunnett's post hoc, HFD vs. HFD-Succ $p = 0.9736$, HFD vs. CC $p = 0.9778$, HFD vs. CC-Succ $p = 0.0447$). (m) Emotionality score (Two-way ANOVA, diet × treatment interaction $p = 0.5805$, treatment $p = 0.002$, diet $p = 0.0004$. Dunnett's post hoc, HFD vs. HFD-Succ $p = 0.1491$, HFD vs. CC $p = 0.088$, HFD vs. CC-Succ $p < 0.0001$). $N = 11$–14/experimental group. Error bars represent SEM. $^{*}p \leq 0.05$, $^{**}p \leq 0.01$ and $^{****}p \leq 0.0001$.

limitations in translating its results to humans, since it imposes larger and more rapid energy switches than those typically experienced by humans undertaking common IF regimens such as time-restricted eating or 5:2 plans. This is caused by species differences in metabolic rate, body size, and mice have relatively higher amounts of metabolically active tissues, such as liver and kidney, and relatively less inactive tissue, such as bone. As a consequence, metabolic switching and ketogenesis occur more rapidly and with greater amplitude in rodents than in humans [56–58]. Nevertheless, although the magnitude of these fluctuations is greater, the fundamental biochemical pathways triggered by IF, such as enhanced fatty-acid oxidation, transient increase in ketone production, and fasting-related molecular signaling, are highly conserved across species [59]. Moreover, our IF protocol did cause a BHB increase, which lies in the nutritional/physiological ketosis range [60]. Thus, although a direct quantitative translation of our findings to human IF regimens should be made with caution, the model remains valuable for investigating fasting-induced metabolic remodeling.

Mice fed a HFD for 14 weeks developed obesity, evidenced by significantly increased BW and impaired glucose tolerance. Among the dietary interventions, the CC-IF regimen was the most effective in reducing both BW and plasma insulin levels compared to HFD-IF and CC alone. This is in line with a recent study conducted in elderly individuals comparing IF and a healthy diet [61]. However, all three regimens successfully restored glucose tolerance. CC-IF also had the most pronounced effect in reducing fat depots. In contrast, the reduction in plasma leptin levels following the dietary switch was comparable across HFD-IF, CC, and CC-IF.

From a translational perspective, these findings suggest that substantial reductions in BW or fat mass may not be required to restore glucose tolerance and lower plasma insulin and leptin levels. Rather, a more moderate weight loss or dietary modulation may suffice to improve key metabolic parameters.

Nonetheless, the liver, a major player in nutrient processing and whole-body metabolic homeostasis [62], displayed specific transcriptional responses to the three different diet switches in comparison to ad libitum HFD feeding. CC-IF had the most dramatic impact with 1537 differentially expressed transcripts, whereas CC and HFD-IF accounted for 463 and 577 DEG, respectively. CC-IF upregulated gene top annotations were related to transcriptional regulation. This is in line with the hepatic tissue tendency to save energy in a condition of limited food and energy resources. Moreover, the liver of the CC-IF, CC, and HFD-IF groups experienced a decrease in the transcription of genes involved in lipid biosynthetic processes, whereas circadian rhythms came up in the annotations of upregulated transcripts. Alterations in liver clock function in response to diet have been previously observed and described as an adaptation mechanism upon a nutritional challenge [63–68]. Although we did not examine daily oscillations in gene expression, our findings suggest that the hepatic clock may play a role in sensing nutritional changes following a dietary switch, independently of the diet-specific composition.

In CC-IF mice, gene sets were significantly enriched for pathways involved in chromatin remodeling, transcriptional regulation, protein trafficking, and DNA repair, mechanisms typically associated with cellular homeostasis and adaptability [49]. In contrast, HFD-IF mice showed enrichment in pathways related to extracellular matrix organization, actin filament dynamics, and responses to mechanical stress, features commonly associated with tissue remodeling and pathological states [69, 70]. These HFD-IF transcriptional signatures may reflect a state of subclinical hepatic inflammation, potentially driven by lipotoxicity [43]. This could be the consequence of prolonged lipid exposure, both from dietary fat during feeding and from adipose tissue mobilization during fasting days. The cyclic overload of lipids may challenge the liver's capacity to maintain lipid homeostasis, ultimately leading to stress responses and inflammation. Thus, although IF may have beneficial effects in the context of a balanced diet, it could exacerbate liver-related metabolic dysfunctions when applied in a HF intake context.

Intriguingly, GO analysis reveals that only CC-IF, not HFD-IF or CC alone, downregulated ubiquitin-proteasome pathway terms in liver and hippocampus—a cascade essential for protein

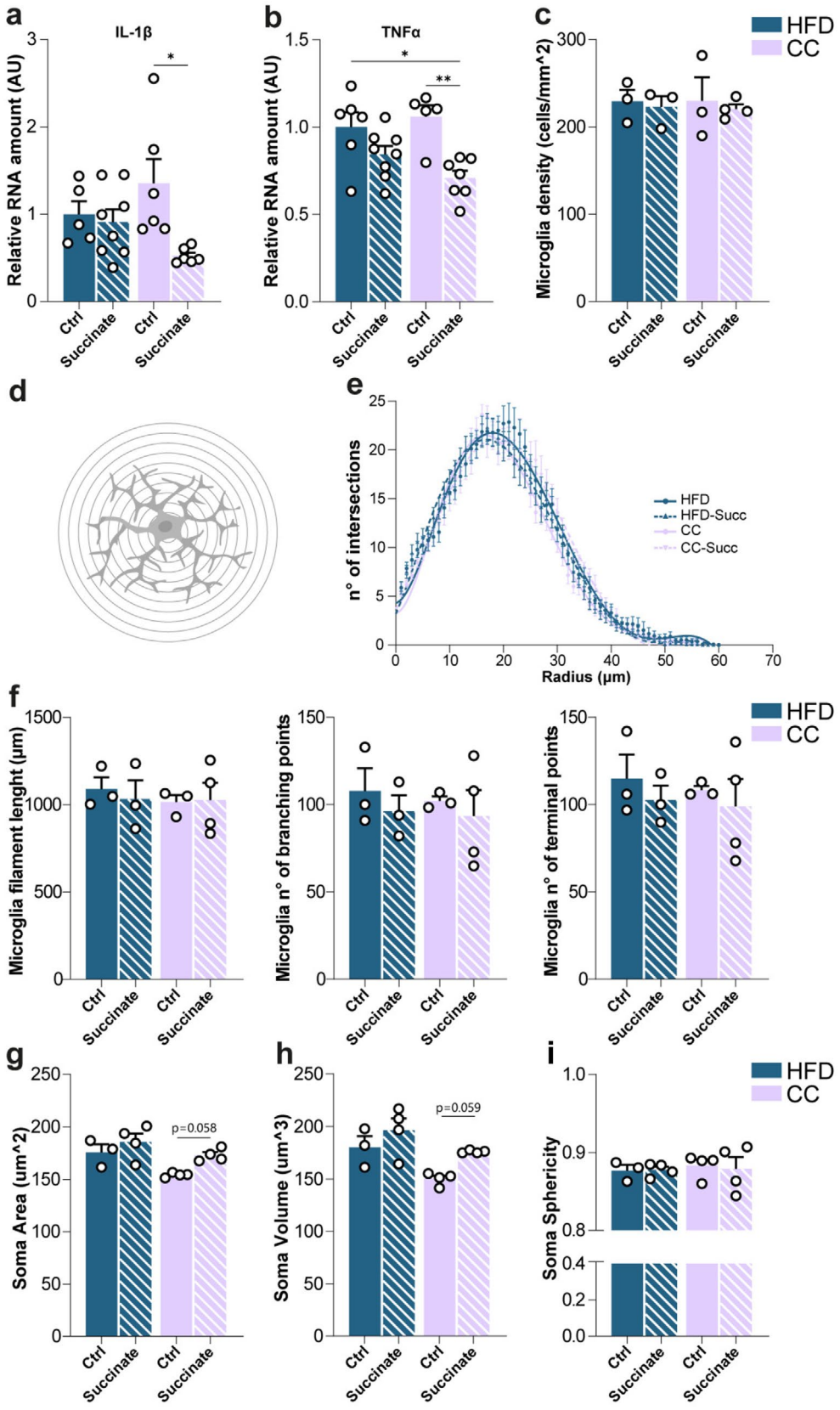

FIGURE 7 | Legend on next page.

homeostasis and cellular quality control [71]. This suggests that the combined intervention featured by CC-IF uniquely reduces the cellular demand for proteolytic clearance, likely reflecting improved proteostasis under this diet.

The CC-IF regimen was particularly effective in improving behavioral outcomes. It was the only intervention that consistently ameliorated both exploratory activity and anxiety-like behavior. Except for unsupported rearing, mice switched to the

FIGURE 7 | Succinate administration affects hippocampal neuroinflammatory markers. (a) IL-1β Relative mRNA expression (Two-way ANOVA, diet × treatment interaction $p = 0.0473$, treatment $p = 0.0168$, diet $p = 0.9293$. Tukey's post hoc, CC vs. CC-Succ $p = 0.0163$). (b) TNFα Relative mRNA expression (Two-way ANOVA, diet × treatment interaction $p = 0.124$, treatment $p = 0.0004$, diet $p = 0.5353$. Tukey's post hoc, HFD vs. CC-Succ $p = 0.0124$, CC vs. CC-Succ $p = 0.004$). (c) Density of hippocampal microglia cells (Two-way ANOVA, diet × treatment interaction $p = 0.9287$, treatment $p = 0.6269$, diet $p = 0.9455$). (d) Representative image of a Sholl analysis for hippocampal microglia reconstruction. (e) Sholl analysis ($n = 14/20$ cells per group. Two-way ANOVA, distance × treatment interaction $p = 0.4595$, distance $p < 0.0001$, treatment $p = 0.5802$). (f) Microglia Filament length (Two-way ANOVA, diet × treatment interaction $p = 0.6954$, treatment $p = 0.795$, diet $p = 0.6602$). *N*° of branching points (Two-way ANOVA, diet × treatment interaction $p = 0.9032$, treatment $p = 0.4183$, diet $p = 0.7261$). *N*° of terminal points (Two-way ANOVA, diet × treatment interaction $p = 0.9095$, treatment $p = 0.4107$, diet $p = 0.6927$). (g) Microglia soma area (Two-way ANOVA, diet × treatment interaction $p = 0.4379$, treatment $p = 0.0251$, diet $p = 0.01$. Sidak's post hoc, HFD vs. HFD-Succ $p = 0.4358$, CC vs. CC-Succ $p = 0.058$). (h) Microglia soma volume (Two-way ANOVA, diet × treatment interaction $p = 0.5314$, treatment $p = 0.0191$, diet $p = 0.0071$. Sidak's post hoc, HFD vs. HFD-Succ $p = 0.3284$, CC vs. CC-Succ $p = 0.0586$). (i) Microglia soma sphericity (Two-way ANOVA, diet × treatment interaction $p = 0.8121$, treatment $p = 0.8647$, diet $p = 0.7008$). $N = 5–8$/group (a, b), $N = 3–4$/group (c–i) Error bars represent SEM. $^{*}p \leq 0.05$ and $^{**}p \leq 0.01$.

CC diet alone did not show significant differences from HFD-fed animals. The HFD-IF group exhibited some improvements in specific parameters within the OF and EPM tests. Previous studies have shown that IF enhances hippocampal plasticity, promoting long-term potentiation and increasing neurogenesis [72, 73], which may ultimately contribute to improved behavioral performance. However, neither BW reduction nor the acute effects of IF alone fully explain the distinct behavioral profiles observed among the experimental groups. The emotionality score further confirmed the superior efficacy of the CC-IF intervention from a behavioral standpoint. Finally, a recent human study showed that IF led to better outcomes than a healthy diet in specific executive function tasks in older adults [61], which may align with our data.

Our metabolites analysis highlighted succinate as a top hit regulated molecule in CC-IF. Intriguingly, succinate was increased in the liver and BAT and decreased in CC-IF plasma. The reduction in circulating succinate could be protective. Elevated plasma or serum succinate concentration has been found in human obesity compared to lean individuals, and the increase seems associated with impaired glucose metabolism [74, 75]. Higher circulating succinate levels consistently correlate with a cluster of established cardiometabolic risk factors, such as BMI, higher fasting insulin, dyslipidemia, increased diastolic blood pressure, and systemic inflammation, as indicated by elevated C-reactive protein [74]. Why CC-IF influences plasma succinate levels is not yet fully understood. However, it may be the most effective regimen for activating thermogenesis, as suggested by the pronounced reduction in BW. CC-IF could promote, through yet unknown mechanisms, the uptake of succinate by BAT [76], where it may be used to stimulate UCP1 activity [51]. On the other hand, the increase in hepatic succinate levels may reflect its role in supporting gluconeogenesis by replenishing TCA cycle intermediates and sustaining the energy demand required for glucose production. CC-IF could be the diet in which a burst in gluconeogenesis is necessary to avoid hypoglycemia. Liver tissue has also been shown to uptake circulating succinate [77, 78]. Interestingly, during exercise and overnight fasting, a significant hepato-splanchnic bed uptake of succinate was observed in human subjects [79], in line with a likely succinate liver uptake upon CC-IF. Finally, we cannot exclude IF mechanisms involving modulation of intestinal [80] or gut microbiota-derived circulating succinate [81]. Thus, the BAT, and potentially the liver, may contribute through a "metabolic vacuum" effect to reduce plasma succinate levels upon CC-IF. Although our findings suggest succinate modulation may serve as a novel metabolic correlate, potentially distinguishing IF from simple caloric restriction, and thereby enhancing the capacity to counteract adiposity, glucose intolerance, and potentially the effect of HFD-induced dysbiosis [75, 82], enhancing a reduction in cardiometabolic risk, they remain associative and do not yet demonstrate causality. Further exploration is necessary to delineate a mechanistic or causal role of succinate modulation in the beneficial effects of IF.

A pivotal aspect of our study was exploring whether the unique succinate signature present in CC-IF mice could be linked to the observed benefits. To test this, we administered sodium succinate in drinking water to DIO mice. Strikingly, succinate supplementation recapitulated several key beneficial outcomes observed in CC-IF. Metabolically, although HFD-Succ mice showed only a slight, non-significant mitigation of HFD-induced weight gain, CC-Succ mice exhibited a significant reduction in BW compared to the CC group, mirroring the enhanced weight loss seen with CC-IF. This suggests that succinate's effect on BW is context-dependent, possibly being more effective when combined with a healthier background diet. Importantly, succinate significantly improved glucose tolerance in HFD-fed mice, aligning with previous studies demonstrating succinate's ability to enhance glucose homeostasis by promoting BAT thermogenesis and energy expenditure [51, 83, 84]. Although Gaspar et al. also showed succinate protects against DIO, our data contrast slightly with Ives et al., who reported reduced adiposity without clear glucose tolerance improvement [85]. The most pronounced improvement in glucose clearance was seen in the CC-Succ group, again paralleling the CC-IF results and suggesting synergy between succinate and a balanced diet. Furthermore, succinate influenced fat depot distribution, particularly BAT weight, consistent with its known role in BAT activation [51, 86].

Behaviorally, succinate supplementation exerted effects remarkably similar to those of CC-IF. Indeed, the emotionality score confirmed that the CC-Succ group significantly reduced anxiety-like behavior compared to the HFD condition, achieving a profile similar to CC-IF mice. Given the links between DIO, neuroinflammation, cognitive decline, and mood disorders [19, 87, 88], we investigated whether succinate could modulate inflammatory markers in the hippocampus. Our transcriptomic analysis in HFD, CC-IF, HFD-IF, and CC hippocampal

tissue revealed that HFD feeding induced pathways related to immune response and neuroinflammation. Notably, succinate supplementation significantly reduced the expression of the pro-inflammatory cytokines IL-1β and TNFα in the hippocampus of CC-Succ mice compared to CC mice, and for TNFα compared to HFD, suggesting a potential anti-inflammatory effect within the brain or a potential indirect effect mediated by improved peripheral metabolism. This finding is particularly interesting given the often-described pro-inflammatory role of succinate accumulation within activated immune cells like macrophages, where it stabilizes HIF-1α and drives IL-1β production [89–91]. However, extracellular succinate signaling via its receptor SUCNR1 can have more complex, context-dependent roles, including anti-inflammatory or resolving actions [82, 90, 92, 93]. Systemic administration, as used here, likely increases circulating succinate, potentially engaging SUCNR1 on various cell types such as neurons, microglia [55], or altering peripheral signals that impact the brain. Our observation aligns with the concept that systemic metabolic shifts (like those induced by IF or potentially succinate supplementation) may dampen central inflammation [88, 94]. Analysis of microglia morphology showed that although switching to the CC diet reduced soma size/volume compared to HFD, succinate tended to increase these parameters, perhaps reflecting an altered activation or metabolic state rather than simple quiescence, warranting further investigation.

In summary, our study demonstrates that systemic succinate supplementation, mimicking certain outcomes of CC-IF, exerts beneficial effects on behavior and reduces inflammatory markers in the hippocampus of DIO mice. The biochemical correlates underlying these effects likely involve a combination of factors: improved peripheral metabolic health indirectly benefiting the brain, and potentially direct central actions, including modulation of inflammatory pathways. Dissecting the relative contributions of these peripheral versus central, and metabolic versus signaling, effects of succinate remains a key area for future investigation. Finally, our study reveals that CC-IF induces body site–specific modulation of succinate, highlighting an associated biochemical remodeling that may underlie its metabolic benefits compared to a balanced ad libitum diet. These findings suggest that IF in individuals with obesity or other metabolic diseases may offer enhanced protection against cardiometabolic risk and reduce the likelihood of developing neuropsychiatric disorders or cognitive dysfunction.

4 | Materials and Methods

4.1 | Animals and Feeding

7–8-week-old male C57BL/6J mice (JAX #00064) were housed (2–3 per cage) in individually ventilated cages in a 12-h light/12-h dark environment at a controlled temperature (23°C). All the mice were initially fed ad libitum a high-fat diet (60% Kcal from fat, irradiated Research Diet #D12492) for 10 weeks and then divided into 4 different feeding groups for the next 4 weeks: a group continuing on the HFD (HFD group), a group practicing IF by consuming the HFD every other day (HFD-IF), a group fed a balanced control chow diet ad libitum (CC, irradiated Research Diet #12450J), and a group practicing IF by consuming the control chow every other day (CC-IF).

At the end of the 14 weeks of dietary regimen, 12 mice/experimental group were sacrificed by decapitation. Half of the animals were used for the RNA extraction experiment, leptin, and insulin OGTT analysis. Half of the animals were used for metabolomics analysis. Hippocampus, liver, subcutaneous fat, perirenal fat, interscapular brown adipose tissue (BAT), and epididymal fat were harvested, snap-frozen in liquid nitrogen, and stored at −80°C until use. Fresh blood was centrifuged at 1500 × g for 15 min, and plasma was isolated and stored at −80°C until use.

4.2 | Oral Glucose Tolerance Test (OGTT)

The OGTT was performed at the end of the 13th week of diet treatment. Before the test, mice were housed in clean cages and fasted for 6 h. Mice were given an oral bolus of glucose (2 g/kg of body weight; D-glucose, Sigma Aldrich Catalog #G6152), and glycemia from tail vein blood samples was quantified through a glucometer (Accu Chek Guide). Glycemia was evaluated at 0, 15, 30, 60, and 120 min post glucose administration.

4.3 | Plasma Insulin and Leptin Levels

Plasma insulin and leptin levels were analyzed using the mouse metabolic hormone panel (Merck Catalog #MMHE-44K), following manufacturer instructions.

4.4 | Behavioral Tests

Behavioral performance was assessed in a dedicated cohort of mice ($n = 8/11$ experimental group). During the last 7 days of diet feeding, mice underwent the open field (OF) test, the novel object recognition test (NORT), the Y maze test, and the elevated plus maze test (EPM).

4.4.1 | Open Field (OF) Test and Novel Object Recognition Test (NORT)

In our battery of tests, the OF has been exploited for the NORT habituation phase.

The apparatus consisted of a square arena (60 × 60 × 30 cm) constructed in poly(vinyl chloride) with black walls and a white floor. The mice received one session of 10-min duration in the empty arena to habituate them to the apparatus and test room. Animal position was continuously recorded by a video tracking system (Noldus Ethovision XT). In the recording software, an area corresponding to the center of the arena (a central square 30 × 30 cm) and a peripheral region (corresponding to the remaining portion of the arena) were defined. The total movement of the animal and the time spent in the center or in the periphery area were automatically computed. Mouse activity during this habituation session was analyzed to evaluate the behavior in the OF arena. Rearing behavior, measured as the number of times an animal temporarily stands on its hindlimbs, was manually counted and used as an exploratory and anxiety-like behavior index [95].

The NORT consisted of two phases: the sample and testing phase. During the sample phase, two identical objects were placed in diagonally opposite corners of the arena, approximately 6 cm from the walls, and mice were allowed to explore the objects for 10 min; then they were returned to their cage. The objects to be discriminated against were made of glass and were too heavy to be displaced by the mice. The testing phase was performed 24 h after the sample phase. One of the two familiar objects was replaced with a new one, and the mice were allowed to explore objects for 5 min. To avoid possible preferences for one of the two objects, the choice of the new and old objects and the position of the new one were randomized among animals. The amount of time spent exploring each object (nose sniffing and head orientation within <2.0 cm) was recorded and evaluated by the Noldus Ethovision XT video tracker system. Arena and objects were cleaned with 70% ethanol between trials to stop the build-up of olfactory cues. A preference index was computed as PI (%) = (T new/(T new + T familiar) × 100), where T new is the time spent exploring the new object, and T familiar is the time spent exploring the old one. Any mouse that explored for less than 13 s was excluded from the analysis.

4.4.2 | Y Maze Test

A Y-shaped maze with three symmetrical gray solid plastic arms at a 120-degree angle (26 cm length, 10 cm width, and 15 cm height) was used to test exploratory and hyperactive behaviors. Mice were placed in the center of the maze and allowed to freely explore the maze for 8 min. The apparatus was carefully cleaned with ethanol between trials to avoid the build-up of odor traces. All sessions were video-recorded (Noldus Ethovision XT) for offline blind analysis. The arm entry is defined as all four limbs within the arm. A triad is defined as a set of three arm entries when each entry is to a different arm of the maze. The number of arm entries and alternate triads were recorded in order to calculate the alternation percentage (generated by dividing the number of alternate triads by the number of total triads and then multiplying by 100), as explained in Ref. [96].

4.4.3 | Elevated Plus Maze (EPM) Test

The plus-shaped arena was installed on a raised support, and a camera (Noldus Ethovision XT) was used to monitor the mice's movements. The arena consisted of a total of four arms: two open and two enclosed by Plexiglas walls (50 cm long and 10 cm wide) with the same illumination levels. Mice were placed in the center of the EPM arena, and exploration was video-tracked for 5 min. Time spent in open and closed arms and frequency of entries were analyzed, as well as the mean velocity and the total distance traveled by each animal. The percentage of time spent in the open arm was evaluated as (T open/(T open + T closed) × 100), where T open is the time spent in the open arm, and T closed is the time spent in the closed arm. The percentage of entries in the open arm was computed as ($N°$ open/($N°$ open + $N°$ closed) × 100), where $N°$ open is the number of entries in the open arm, and $N°$ closed is the number of entries in the closed arm. The EPM arena was cleaned with 70% ethanol between each trial. Mice that fell from the platform were excluded from the analysis.

The emotionality score was calculated as explained in Ref. [47]. It was derived by averaging the z-scores of four parameters: time spent in the center (#1) and the number of total rears (#2) in the OF test, along with percentage of time spent (#3) and the percentage of number of entries (#4) in the open arm during the EPM. Animals that were excluded from the behavioral tests used for calculation of the emotionality score were also excluded from the score.

4.5 | RNA Extraction

Hippocampus and liver samples were homogenized in phenol/guanidine-based QIAzol Lysis Reagent (Qiagen #79306). Chloroform was added, and the samples were shaken for 15 s. The samples were left at 20°C–24°C for 3 min and then centrifuged (12 000 × g, 20 min, 4°C). The upper phase aqueous solution, containing RNA, was collected in a fresh tube, and the RNA was precipitated by the addition of isopropanol. Samples were mixed by vortexing, left at RT for 10 min, and then centrifuged (12 000 × g, 15 min, 4°C). The supernatant was discarded, and the RNA pellet was washed in 75% ethanol by centrifugation (7500 × g, 5 min, 4°C). The supernatant was discarded, and the pellet was left to dry for a minimum of 15 min before resuspending in RNAse-free water.

RNA concentration was determined by the Nanodrop Spectrophotometer (Thermoscientific 2000 C). RNA quality was analyzed via agarose gel electrophoresis (1% agarose).

4.6 | qPCR

Total RNA was reverse transcribed using QuantiTech Reverse Transcription Kit (Qiagen Cat. # 205311). Gene expression was analyzed by real-time PCR (Step One, Applied Biosystems), using PowerUp SYBR Green Master Mix (Thermo Fisher #A25742). The primers for gene expression were designed by Primer 3 software (v. 0.4.0), and are reported below:

Actb: Forward: 5′-GGCTGTATTCCCCTCCATGC-3′;

Actb: Reverse: 5′-CCAGTTGGTAACAATGCCATGT-3′;

Tnfα: Forward: 5′-CCCATATACCTGGGAGGAGTCTTC-3′;

Tnfα: Reverse: 5′-CATTCCCTTCACAGAGCAATGAC-3′;

Il1β: Forward: 5′-AGTTGACGGACCCCAAAAG-3′;

Il1β: Reverse: 5′-AGCTGGATGCTCTCATCAGG-3′.

Quantitative values for cDNA amplification were calculated from the threshold cycle number (Ct) obtained during the exponential growth of the PCR products. Threshold was set automatically by the Step One software. Data were analyzed by the ΔΔCt methods using the *actb* expression to normalize the cDNA levels of the transcripts under investigation.

4.7 | RNA Sequencing (Seq)

Library preparation and RNA-seq technique were performed by a commercially available service (IGATech Udine, Italy). Total RNA was extracted as described above, libraries were prepared and sequenced on Illumina HiSeq2500 instrument during a pair-end read 125 bp sequencing, producing sequencing results in FastQ format. The FastQ files were processed through the standard Tuxedo protocol, using Tophat and Cufflinks. Tophat was used to align the RNA-seq reads to the reference genome assembly mm10 and Cufflinks was used to calculate gene expression levels. This protocol outputs the FPKM values for each gene of each replicate.

The differential analysis of the FPKM values across all experiments and control groups was conducted with Cyber-T, a differential analysis program using a Bayesian-regularized *t*-test [97, 98]. The *p*-value thresholds used to determine differential expression were 0.05 for the liver and 0.1 for the hippocampus.

4.8 | Gene Ontology Analysis

Gene ontology analysis was performed using Database for Annotation, Visualization and Integrated Discovery (DAVID) v6.7, using genomic background; GO Biological Processes were chosen for gene clustering.

4.9 | Metabolomics

Polar metabolites were quantified in 40 μL of plasma and in about 20 mg of liver, hippocampus, and brown adipose tissue (BAT). Tissues were homogenized using Precellys Evolution Homogenizer (Bertin Instruments, Frankfurt, Germany). Samples were deproteinized with methanol by centrifugation for 20 min at 13 300 rpm at 4°C, and metabolites were extracted by a modified Folch method [99] using chloroform: methanol (2:1) and water, after 15 min of centrifugation at 13 300 rpm at 4°C. Upper phases were dried under gentle nitrogen flux and were derivatized using 10 μL of methoxyamine hydrochloride (Merck KGaA, Darmstadt, Germany) solution in pyridine (20 mg/mL) for 30 min at 60°C and 30 μL of N-(tert-butyldimethylsilyl)-N-methyltrifluoroacetamide (TBDMS, Merck KGaA, Darmstadt, Germany) with 70 μL acetonitrile for 1 h at 60°C. Amino acids and organic acids were quantified using labeled internal standard mix (MSK-A2-S Metabolomics Amino Acid Mix standard, CIL Cambridge, MA, USA, and MSK-OA-1 Labeled Organic Acid Mix, CIL Cambridge, MA, USA) and measured by gas chromatography/tandem mass spectrometry (GC 8890/MS 7000D, Agilent, Santa Clara, CA).

4.10 | Succinate Treatment

A dedicated cohort of 7–8 week-old male C57BL/6J mice was initially fed ad libitum a HFD for 10 weeks and then divided into 4 different groups for the next 4 weeks: a group continuing on the HFD (HFD), a group consuming HFD and drinking Succinate (HFD-Succ), a group fed a CC diet ad libitum (CC), and a group consuming CC and drinking Succinate (CC-Succ). Sodium succinate (Sigma Aldrich #224731) was dissolved in drinking water (1.5% w/vol) and refreshed every 2 days. A total of 11–14 mice/experimental groups were used in this experiment. Half of the animals were sacrificed, and fresh tissues were collected. Half of the animals were transcardially perfused.

4.11 | Microglia Immunofluorescence Analysis

Mice were anesthetized with chloral hydrate (20 mL/kg BW) and perfused via intracardiac infusion with PBS and then 4% paraformaldehyde (PFA, w/vol, dissolved in 0.1 M phosphate buffer, pH 7.4). Brains were quickly removed and post-fixed overnight in PFA at 4°C, then transferred to a 30% sucrose (w/vol) solution. 45 μm coronal sections were cut on a freezing microtome (Leica), and free-floating sections were processed for immunofluorescence.

Hippocampal sections were incubated for 2 h in a blocking solution containing 10% BSA (w/vol) and 0.5% Triton X-100 (vol/vol) in PBS and incubated overnight at 4°C with guinea pig anti-iba1 (Synaptic Systems # 234308) diluted 1:500 in PBS with 3% BSA (w/vol) and 0.15% Triton X-100 (vol/vol).

Sections were then washed with PBS and incubated for 2 h at 22°C–24°C with Alexa Fluor 488–conjugated secondary antibody (Invitrogen # A-11073), which was added at a dilution of 1:500 in the same solution as the primary antibody.

Sections were washed three times with PBS and mounted on slides; then they were air-dried and coverslipped with Vectashield mounting medium (Vector Laboratories, Cat. no. H-1000). Imaging was performed on a Leica STELLARIS 5 confocal microscope (Leica Microsystems, Wetzlar, Germany) using a dry 20× and a 63× oil objective. The area of the hippocampus was defined on the basis of the mouse brain atlas (Paxinos and Franklin's The Mouse Brain in Stereotaxic Coordinates).

IBA1-positive cell counting for microglia density analysis was performed using a custom MATLAB-based graphical user interface [100].

The 3D reconstruction of microglial cells was performed on Z-stacks of ~45 μm, acquired with a z-step of 0.50 μm (for a final voxel size of 0.12025 × 0.12025 × 0.5 μm). Images were then processed for filament and soma reconstruction using, respectively, the "Filaments" and "Surfaces" functions of IMARIS software (Bitplane). The analyzed morphological features were selected on the basis of their relevance as indicators of microglia activation: filament length, number of branching points, number of terminal points, soma area, soma volume, and soma sphericity (roundness) [96, 101].

Between 4 and 7 microglia cells per mouse were reconstructed for the arborization analysis. Between 7 and 11 cells were used for the soma analysis.

4.12 | Statistical Analysis

The sample sizes (*n*) were based on prior studies and are indicated in the figure legend for each panel. Whenever possible, quantification and analyses were performed blind to the

experimental condition. The reported "n" refers to individual animals, and each circle over the graph bars represents a single mouse, unless otherwise stated.

Most statistical analyses were performed using GraphPad Prism version 7 (GraphPad Software, San Diego, CA, USA). Outliers were identified using the Grubbs' test for single outliers, with a significance level set at $\alpha = 0.05$. The intergroup difference was determined by two-way analysis of variance (ANOVA), followed by Sidak's or Tukey's post hoc correction for multiple comparisons, as specified in each figure legend. Although statistical correction was applied, we acknowledge that the sample size (8–11 animals per group) may not completely exclude the risk of type I errors (false positives) in behavioral datasets.

Only the p values of statistically significant post hoc comparisons are reported in the figure legend. All data are represented as the mean ± SEM. p values of ≤ 0.05 were considered statistically significant, and significance was defined in the figure panels as follows: $^{*}p \leq 0.05$, $^{**}p \leq 0.01$, and $^{***}p \leq 0.001$, $^{****}p \leq 0.0001$.

Author Contributions

A.T. performed all the experiments, analyzed the data, and prepared the figures. F.C. performed all the metabolome analysis and analyzed the data. S.A. and K.C.A. performed the RNA-seq analysis. S.C., M.G.G., A.M., F.D., and M.N. helped with tissue collection, behavioral, and molecular/immunofluorescence experiments. L.D.B. quantified succinate in BAT. G.S. and M.M. collected adipose tissues. P.B. supervised the RNA-seq analysis and interpreted the data. A.G. supervised, analyzed, and interpreted the metabolomics. M.M., A.G., and P.B. gave feedback on the manuscript. P.T. and A.G. conceived the project. P.T. designed, supervised, and performed the experiments, interpreted the data, and wrote the manuscript. A.T. and P.T. performed the manuscript revision.

Acknowledgments

We thank the members of Tognini's team for insightful comments and feedback. Special thanks to Giulia Tiozzo for her help with succinate experiments, to Sara and Cecilia Ciampi, and Dr. Silvia Burchielli for their help in the mouse facility.

Funding

This research was in part funded under the National Recovery and Resilience Plan (PNRR), Mission 4 Component 2 Investment 3.1 of the Italian Ministry of University and Research funded by the European Union—NextGenerationEU, "Biorobotics Research and Innovation Engineering Facilities" project (Project identification code IR0000036—CUP J13C22000400007); PNRR YOUNG MSCA_0000081 iNsPIReD, and PRIN-PNRR2022 CARE P2022CXN7X CUP I53D23006920001 to P.T; in part through an EFSD award supported by EFSD/Lilly European Diabetes Research Programme to AG and PT, and in part funded by the European Union, grant agreement No 101080329 (Project PAS GRAS) to AG. Views and opinions expressed are, however, those of the author(s) only and do not necessarily reflect those of the European Union or European Health and Digital Executive Agency (HADEA), under the powers delegated by the European Commission.

Ethics Statement

All the experiments were carried out in accordance with the European Directives (2010/63/EU) and were approved by the Italian Ministry of Health.

Conflicts of Interest

The authors declare no conflicts of interest.

Data Availability Statement

RNA-seq data generated in this study has been deposited in the NCBI Gene Expression Omnibus (GEO) database, GEO accession number GSE298120. The algorithms used for microglia density data analysis have been published at Zenodo DOI: 10.5281/zenodo.14761458. Any additional information required to reanalyze the data reported in this paper is available from the lead contact upon request.

References

1. S. Kloock, C. G. Ziegler, and U. Dischinger, "Obesity and Its Comorbidities, Current Treatment Options and Future Perspectives: Challenging Bariatric Surgery?," *Pharmacology & Therapeutics* 251 (2023): 108549.

2. T. M. Powell-Wiley, P. Poirier, L. E. Burke, et al., "Obesity and Cardiovascular Disease: A Scientific Statement From the American Heart Association," *Circulation* 143 (2021): e984–e1010.

3. T. Scully, A. Ettela, D. LeRoith, and E. J. Gallagher, "Obesity, Type 2 Diabetes, and Cancer Risk," *Frontiers in Oncology* 10 (2020): 615375.

4. F. Morys, O. Potvin, Y. Zeighami, et al., "Obesity-Associated Neurodegeneration Pattern Mimics Alzheimer's Disease in an Observational Cohort Study," *Journal of Alzheimer's Disease* 91 (2023): 1059–1071.

5. R. A. Whitmer, D. R. Gustafson, E. Barrett-Connor, M. N. Haan, E. P. Gunderson, and K. Yaffe, "Central Obesity and Increased Risk of Dementia More Than Three Decades Later," *Neurology* 71 (2008): 1057–1064.

6. P. Li, X. Zhu, C. Huang, et al., "Effects of Obesity on Aging Brain and Cognitive Decline: A Cohort Study From the UK Biobank," *IBRO Neuroscience Reports* 18 (2025): 148–157.

7. L. B. Hassing, A. K. Dahl, N. L. Pedersen, and B. Johansson, "Overweight in Midlife Is Related to Lower Cognitive Function 30 Years Later: A Prospective Study With Longitudinal Assessments," *Dementia and Geriatric Cognitive Disorders* 29 (2010): 543–552.

8. J. Gunstad, R. H. Paul, R. A. Cohen, D. F. Tate, M. B. Spitznagel, and E. Gordon, "Elevated Body Mass Index Is Associated With Executive Dysfunction in Otherwise Healthy Adults," *Comprehensive Psychiatry* 48 (2007): 57–61.

9. R. E. Mrak, "Alzheimer-Type Neuropathological Changes in Morbidly Obese Elderly Individuals," *Clinical Neuropathology* 28 (2009): 40–45.

10. A. G. Lentoor, "Obesity and Neurocognitive Performance of Memory, Attention, and Executive Function," *NeuroSci* 3 (2022): 376–386.

11. X. Tang, W. Zhao, M. Lu, et al., "Relationship Between Central Obesity and the Incidence of Cognitive Impairment and Dementia From Cohort Studies Involving 5,060,687 Participants," *Neuroscience and Biobehavioral Reviews* 130 (2021): 301–313.

12. L. G. Cheke, J. S. Simons, and N. S. Clayton, "Higher Body Mass Index Is Associated With Episodic Memory Deficits in Young Adults," *Quarterly Journal of Experimental Psychology (Hove)* 69 (2016): 2305–2316.

13. H. L. Sargénius, S. Lydersen, and K. Hestad, "Neuropsychological Function in Individuals With Morbid Obesity: A Cross-Sectional Study," *BMC Obesity* 4 (2017): 6.

14. J. C. D. Nguyen, A. S. Killcross, and T. A. Jenkins, "Obesity and Cognitive Decline: Role of Inflammation and Vascular Changes," *Frontiers in Neuroscience* 8 (2014): 375.

15. J. S. Laurent, R. Watts, S. Adise, et al., "Associations Among Body Mass Index, Cortical Thickness, and Executive Function in Children," *JAMA Pediatrics* 174 (2020): 170–177.

16. N. Medic, H. Ziauddeen, K. D. Ersche, et al., "Increased Body Mass Index Is Associated With Specific Regional Alterations in Brain Structure," *International Journal of Obesity (London)* 40 (2016): 1177–1182.

17. J. F. Bobb, B. S. Schwartz, C. Davatzikos, and B. Caffo, "Cross-Sectional and Longitudinal Association of Body Mass Index and Brain Volume," *Human Brain Mapping* 35 (2014): 75–88.

18. F. Kurth, J. G. Levitt, O. R. Phillips, et al., "Relationships Between Gray Matter, Body Mass Index, and Waist Circumference in Healthy Adults," *Human Brain Mapping* 34 (2013): 1737–1746.

19. S. Dutheil, K. T. Ota, E. S. Wohleb, K. Rasmussen, and R. S. Duman, "High-Fat Diet Induced Anxiety and Anhedonia: Impact on Brain Homeostasis and Inflammation," *Neuropsychopharmacology* 41 (2016): 1874–1887.

20. P. M. Dingess, R. A. Darling, E. Kurt Dolence, B. W. Culver, and T. E. Brown, "Exposure to a Diet High in Fat Attenuates Dendritic Spine Density in the Medial Prefrontal Cortex," *Brain Structure & Function* 222 (2017): 1077–1085.

21. K. Lyall, K. L. Munger, É. J. O'Reilly, S. L. Santangelo, and A. Ascherio, "Maternal Dietary Fat Intake in Association With Autism Spectrum Disorders," *American Journal of Epidemiology* 178 (2013): 209–220.

22. C. André, A.-L. Dinel, G. Ferreira, S. Layé, and N. Castanon, "Diet-Induced Obesity Progressively Alters Cognition, Anxiety-Like Behavior and Lipopolysaccharide-Induced Depressive-Like Behavior: Focus on Brain Indoleamine 2,3-Dioxygenase Activation," *Brain, Behavior, and Immunity* 41 (2014): 10–21, https://doi.org/10.1016/j.bbi.2014.03.012.

23. M. Solas, F. I. Milagro, M. J. Ramírez, and J. Alfredo Martínez, "Inflammation and Gut-Brain Axis Link Obesity to Cognitive Dysfunction: Plausible Pharmacological Interventions," *Current Opinion in Pharmacology* 37 (2017): 87–92, https://doi.org/10.1016/j.coph.2017.10.005.

24. Z. A. Cordner and K. L. K. Tamashiro, "Effects of High-Fat Diet Exposure on Learning & Memory," *Physiology & Behavior* 152 (2015): 363–371, https://doi.org/10.1016/j.physbeh.2015.06.008.

25. B. L. Tan and M. E. Norhaizan, "Effect of High-Fat Diets on Oxidative Stress, Cellular Inflammatory Response and Cognitive Function," *Nutrients* 11 (2019): 2579, https://doi.org/10.3390/nu11112579.

26. V. D. Longo and M. P. Mattson, "Fasting: Molecular Mechanisms and Clinical Applications," *Cell Metabolism* 19 (2014): 181–192.

27. X. Yuan, J. Wang, S. Yang, et al., "Effect of Intermittent Fasting Diet on Glucose and Lipid Metabolism and Insulin Resistance in Patients With Impaired Glucose and Lipid Metabolism: A Systematic Review and Meta-Analysis," *International Journal of Endocrinology* 2022 (2022): 6999907.

28. R. Antoni, K. L. Johnston, A. L. Collins, and M. D. Robertson, "Effects of Intermittent Fasting on Glucose and Lipid Metabolism," *Proceedings of the Nutrition Society* 76 (2017): 361–368.

29. N. Halberg, M. Henriksen, N. Söderhamn, et al., "Effect of Intermittent Fasting and Refeeding on Insulin Action in Healthy Men," *Journal of Applied Physiology (1985)* 99 (2005): 2128–2136.

30. L. K. Heilbronn, A. E. Civitarese, I. Bogacka, S. R. Smith, M. Hulver, and E. Ravussin, "Glucose Tolerance and Skeletal Muscle Gene Expression in Response to Alternate Day Fasting," *Obesity Research* 13 (2005): 574–581.

31. L. K. Heilbronn, S. R. Smith, C. K. Martin, S. D. Anton, and E. Ravussin, "Alternate-Day Fasting in Nonobese Subjects: Effects on Body Weight, Body Composition, and Energy Metabolism," *American Journal of Clinical Nutrition* 81 (2005): 69–73.

32. J. Ma, Y. Cheng, Q. Su, et al., "Effects of Intermittent Fasting on Liver Physiology and Metabolism in Mice," *Experimental and Therapeutic Medicine* 22 (2021): 950.

33. A. Di Francesco, A. G. Deighan, L. Litichevskiy, et al., "Dietary Restriction Impacts Health and Lifespan of Genetically Diverse Mice," *Nature* 634 (2024): 684–692.

34. O. Strilbytska, S. Klishch, K. B. Storey, A. Koliada, and O. Lushchak, "Intermittent Fasting and Longevity: From Animal Models to Implication for Humans," *Ageing Research Reviews* 96 (2024): 102274.

35. J. Lee, W. Duan, and M. P. Mattson, "Evidence That Brain-Derived Neurotrophic Factor Is Required for Basal Neurogenesis and Mediates, in Part, the Enhancement of Neurogenesis by Dietary Restriction in the Hippocampus of Adult Mice," *Journal of Neurochemistry* 82 (2002): 1367–1375.

36. C. Vivar, M. C. Potter, J. Choi, et al., "Monosynaptic Inputs to New Neurons in the Dentate Gyrus," *Nature Communications* 3 (2012): 1107.

37. Y. Zhao, M. Jia, W. Chen, and Z. Liu, "The Neuroprotective Effects of Intermittent Fasting on Brain Aging and Neurodegenerative Diseases via Regulating Mitochondrial Function," *Free Radical Biology and Medicine* 182 (2022): 206–218.

38. L. Murta, D. Seixas, L. Harada, R. F. Damiano, and M. Zanetti, "Intermittent Fasting as a Potential Therapeutic Instrument for Major Depression Disorder: A Systematic Review of Clinical and Preclinical Studies," *International Journal of Molecular Sciences* 24 (2023): 15551, https://doi.org/10.3390/ijms242115551.

39. R. B. Carteri, L. N. Menegassi, M. Feldmann, et al., "Intermittent Fasting Promotes Anxiolytic-Like Effects Unrelated to Synaptic Mitochondrial Function and BDNF Support," *Behavioural Brain Research* 404 (2021): 113163.

40. R. Fernández-Rodríguez, V. Martínez-Vizcaíno, A. E. Mesas, B. Notario-Pacheco, M. Medrano, and L. K. Heilbronn, "Does Intermittent Fasting Impact Mental Disorders? A Systematic Review With Meta-Analysis," *Critical Reviews in Food Science and Nutrition* 63 (2023): 11169–11184.

41. S. Cornuti, S. Chen, L. Lupori, et al., "Brain Histone Beta-Hydroxybutyrylation Couples Metabolism With Gene Expression," *Cellular and Molecular Life Sciences* 80 (2023): 28.

42. K. Lois and S. Kumar, "Obesity and Diabetes," *Endocrinología y Nutrición* 56S4 (2009): 38–42.

43. G. Mocciaro and A. Gastaldelli, "Obesity-Related Insulin Resistance: The Central Role of Adipose Tissue Dysfunction," *Handbook of Experimental Pharmacology* 274 (2022): 145–164.

44. R. C. Frederich, A. Hamann, S. Anderson, B. Löllmann, B. B. Lowell, and J. S. Flier, "Leptin Levels Reflect Body Lipid Content in Mice: Evidence for Diet-Induced Resistance to Leptin Action," *Nature Medicine* 1 (1995): 1311–1314.

45. N. Castanon, J. Lasselin, and L. Capuron, "Neuropsychiatric Comorbidity in Obesity: Role of Inflammatory Processes," *Frontiers in Endocrinology* 5 (2014): 74.

46. O. Sturman, P.-L. Germain, and J. Bohacek, "Exploratory Rearing: A Context- and Stress-Sensitive Behavior Recorded in the Open-Field Test," *Stress (Amsterdam, Netherlands)* 21 (2018): 443–452.

47. J.-P. Guilloux, M. Seney, N. Edgar, and E. Sibille, "Integrated Behavioral z-Scoring Increases the Sensitivity and Reliability of Behavioral Phenotyping in Mice: Relevance to Emotionality and Sex," *Journal of Neuroscience Methods* 197 (2011): 21–31.

48. M. Murakami and P. Tognini, "Molecular Mechanisms Underlying the Bioactive Properties of a Ketogenic Diet," *Nutrients* 14 (2022): 782, https://doi.org/10.3390/nu14040782.

49. C. E. Geisler, C. Hepler, M. R. Higgins, and B. J. Renquist, "Hepatic Adaptations to Maintain Metabolic Homeostasis in Response to Fasting and Refeeding in Mice," *Nutrition & Metabolism* 13 (2016): 62.

50. S. Satapati, N. E. Sunny, B. Kucejova, et al., "Elevated TCA Cycle Function in the Pathology of Diet-Induced Hepatic Insulin Resistance and Fatty Liver," *Journal of Lipid Research* 53 (2012): 1080–1092.

51. E. L. Mills, K. A. Pierce, M. P. Jedrychowski, et al., "Accumulation of Succinate Controls Activation of Adipose Tissue Thermogenesis," *Nature* 560 (2018): 102–106.

52. S. Fernández-Veledo, A. Marsal-Beltran, and J. Vendrell, "Type 2 Diabetes and Succinate: Unmasking an Age-Old Molecule," *Diabetologia* 67 (2024): 430–442.

53. L. Muzio, A. Viotti, and G. Martino, "Microglia in Neuroinflammation and Neurodegeneration: From Understanding to Therapy," *Frontiers in Neuroscience* 15 (2021): 742065.

54. K. Biswas, "Microglia Mediated Neuroinflammation in Neurodegenerative Diseases: A Review on the Cell Signaling Pathways Involved in Microglial Activation," *Journal of Neuroimmunology* 383 (2023): 578180.

55. L. Wang, Y. Zhang, M. Kiprowska, Y. Guo, K. Yamamoto, and X. Li, "Diethyl Succinate Modulates Microglial Polarization and Activation by Reducing Mitochondrial Fission and Cellular ROS," *Metabolites* 11 (2021): 854, https://doi.org/10.3390/metabo11120854.

56. R. L. Perlman, "Mouse Models of Human Disease: An Evolutionary Perspective," *Evolution, Medicine, and Public Health* 2016 (2016): 170–176.

57. M. L. Reitman, "Of Mice and Men—Environmental Temperature, Body Temperature, and Treatment of Obesity," *FEBS Letters* 592 (2018): 2098–2107.

58. T. Esposito and S. Cortellino, "Calorie Restriction and Periodic Fasting From Rodent to Human: Lost in Translation?," *Annals of Research in Oncology* 4 (2024): 40.

59. V. D. Longo, M. Di Tano, M. P. Mattson, and N. Guidi, "Intermittent and Periodic Fasting, Longevity and Disease," *Nature Aging* 1 (2021): 47–59.

60. C. Fante, F. Spritzler, L. Calabrese, N. Laurent, C. Roberts, and S. Deloudi, "The Role of β-Hydroxybutyrate Testing in Ketogenic Metabolic Therapies," *Frontiers in Nutrition* 12 (2025): 1629921.

61. D. Kapogiannis, A. Manolopoulos, R. Mullins, et al., "Brain Responses to Intermittent Fasting and the Healthy Living Diet in Older Adults," *Cell Metabolism* 36 (2024): 1668–1678.e5.

62. L. Bideyan, R. Nagari, and P. Tontonoz, "Hepatic Transcriptional Responses to Fasting and Feeding," *Genes & Development* 35 (2021): 635–657.

63. P. Tognini, M. Murakami, Y. Liu, et al., "Distinct Circadian Signatures in Liver and Gut Clocks Revealed by Ketogenic Diet," *Cell Metabolism* 26 (2017): 523–538.e5.

64. K. L. Eckel-Mahan, V. R. Patel, S. de Mateo, et al., "Reprogramming of the Circadian Clock by Nutritional Challenge," *Cell* 155 (2013): 1464–1478.

65. M. Murakami, P. Tognini, Y. Liu, K. L. Eckel-Mahan, P. Baldi, and P. Sassone-Corsi, "Gut Microbiota Directs PPARγ-Driven Reprogramming of the Liver Circadian Clock by Nutritional Challenge," *EMBO Reports* 17 (2016): 1292–1303.

66. C. Vollmers, S. Gill, L. DiTacchio, S. R. Pulivarthy, H. D. Le, and S. Panda, "Time of Feeding and the Intrinsic Circadian Clock Drive Rhythms in Hepatic Gene Expression," *Proceedings of the National Academy of Sciences of the United States of America* 106 (2009): 21453–21458.

67. A. Kohsaka, A. D. Laposky, K. M. Ramsey, et al., "High-Fat Diet Disrupts Behavioral and Molecular Circadian Rhythms in Mice," *Cell Metabolism* 6 (2007): 414–421.

68. K. Kinouchi, C. Magnan, N. Ceglia, et al., "Fasting Imparts a Switch to Alternative Daily Pathways in Liver and Muscle," *Cell Reports* 25 (2018): 3299–3314.e6.

69. C. Ortiz, R. Schierwagen, L. Schaefer, S. Klein, X. Trepat, and J. Trebicka, "Extracellular Matrix Remodeling in Chronic Liver Disease," *Current Tissue Microenvironment Reports* 2 (2021): 41–52.

70. P. Bedossa and V. Paradis, "Liver Extracellular Matrix in Health and Disease," *Journal of Pathology* 200 (2003): 504–515.

71. F. Shang and A. Taylor, "Ubiquitin-Proteasome Pathway and Cellular Responses to Oxidative Stress," *Free Radical Biology & Medicine* 51 (2011): 5–16.

72. S.-H. Baik, V. Rajeev, D. Y.-W. Fann, D.-G. Jo, and T. V. Arumugam, "Intermittent Fasting Increases Adult Hippocampal Neurogenesis," *Brain and Behavior* 10 (2020): e01444.

73. J. Beveridge, A. Montgomery, and G. Grossberg, "Intermittent Fasting and Neurocognitive Disorders: What the Evidence Shows," *Journal of Nutrition, Health & Aging* 29 (2025): 100480.

74. F. J. Osuna-Prieto, B. Martinez-Tellez, L. Ortiz-Alvarez, et al., "Elevated Plasma Succinate Levels Are Linked to Higher Cardiovascular Disease Risk Factors in Young Adults," *Cardiovascular Diabetology* 20 (2021): 151.

75. C. Serena, V. Ceperuelo-Mallafré, N. Keiran, et al., "Elevated Circulating Levels of Succinate in Human Obesity Are Linked to Specific Gut Microbiota," *ISME Journal* 12 (2018): 1642–1657.

76. A. Reddy, S. Winther, N. Tran, et al., "Monocarboxylate Transporters Facilitate Succinate Uptake Into Brown Adipocytes," *Nature Metabolism* 6 (2024): 567–577.

77. R. Hems, M. Stubbs, and H. A. Krebs, "Restricted Permeability of Rat Liver for Glutamate and Succinate," *Biochemical Journal* 107 (1968): 807–815.

78. N. Poupin, M. Tremblay-Franco, A. Amiel, et al., "Arterio-Venous Metabolomics Exploration Reveals Major Changes Across Liver and Intestine in the Obese Yucatan Minipig," *Scientific Reports* 9 (2019): 12527.

79. C. Hu, M. Hoene, P. Plomgaard, et al., "Muscle-Liver Substrate Fluxes in Exercising Humans and Potential Effects on Hepatic Metabolism," *Journal of Clinical Endocrinology and Metabolism* 105 (2020): 1196–1209.

80. W. Tong, S. A. Hannou, Y. Wang, et al., "The Intestine Is a Major Contributor to Circulating Succinate in Mice," *FASEB Journal* 36 (2022): e22546.

81. Y.-H. Wei, X. Ma, J.-C. Zhao, X.-Q. Wang, and C.-Q. Gao, "Succinate Metabolism and Its Regulation of Host-Microbe Interactions," *Gut Microbes* 15 (2023): 2190300.

82. S. Fernández-Veledo and J. Vendrell, "Gut Microbiota-Derived Succinate: Friend or Foe in Human Metabolic Diseases?," *Reviews in Endocrine and Metabolic Disorders* 20 (2019): 439–447.

83. R. S. Gaspar, J. Delafiori, G. Zuccoli, et al., "Exogenous Succinate Impacts Mouse Brown Adipose Tissue Mitochondrial Proteome and Potentiates Body Mass Reduction Induced by Liraglutide," *American Journal of Physiology. Endocrinology and Metabolism* 324 (2023): E226–E240.

84. F.-H. Liao, C.-N. Yao, S.-P. Chen, T.-H. Wu, and S.-Y. Lin, "Transdermal Delivery of Succinate Accelerates Energy Dissipation of Brown Adipocytes to Reduce Remote Fat Accumulation," *Molecular Pharmaceutics* 19 (2022): 4299–4310.

85. S. J. Ives, K. S. Zaleski, C. Slocum, et al., "The Effect of Succinic Acid on the Metabolic Profile in High-Fat Diet-Induced Obesity and Insulin Resistance," *Physiological Reports* 8 (2020): e14630.

86. E. L. Mills, C. Harmon, M. P. Jedrychowski, et al., "UCP1 Governs Liver Extracellular Succinate and Inflammatory Pathogenesis," *Nature Metabolism* 3 (2021): 604–617.

87. P. J. Pistell, C. D. Morrison, S. Gupta, et al., "Cognitive Impairment Following High Fat Diet Consumption Is Associated With Brain Inflammation," *Journal of Neuroimmunology* 219 (2010): 25–32.

88. G. Cavaliere, G. Trinchese, E. Penna, et al., "High-Fat Diet Induces Neuroinflammation and Mitochondrial Impairment in Mice Cerebral Cortex and Synaptic Fraction," *Frontiers in Cellular Neuroscience* 13 (2019): 509.

89. E. Mills and L. A. J. O'Neill, "Succinate: A Metabolic Signal in Inflammation," *Trends in Cell Biology* 24 (2014): 313–320.

90. H. Huang, G. Li, Y. He, et al., "Cellular Succinate Metabolism and Signaling in Inflammation: Implications for Therapeutic Intervention," *Frontiers in Immunology* 15 (2024): 1404441.

91. G. M. Tannahill, A. M. Curtis, J. Adamik, et al., "Succinate Is an Inflammatory Signal That Induces IL-1β Through HIF-1α," *Nature* 496 (2013): 238–242.

92. N. Keiran, V. Ceperuelo-Mallafré, E. Calvo, et al., "SUCNR1 Controls an Anti-Inflammatory Program in Macrophages to Regulate the Metabolic Response to Obesity," *Nature Immunology* 20 (2019): 581–592.

93. L. Peruzzotti-Jametti, J. D. Bernstock, N. Vicario, et al., "Macrophage-Derived Extracellular Succinate Licenses Neural Stem Cells to Suppress Chronic Neuroinflammation," *Cell Stem Cell* 22 (2018): 355–368.e13.

94. O. Guillemot-Legris, J. Masquelier, A. Everard, P. D. Cani, M. Alhouayek, and G. G. Muccioli, "High-Fat Diet Feeding Differentially Affects the Development of Inflammation in the Central Nervous System," *Journal of Neuroinflammation* 13 (2016): 206.

95. C. Lever, S. Burton, and J. O'Keefe, "Rearing on Hind Legs, Environmental Novelty, and the Hippocampal Formation," *Reviews in the Neurosciences* 17 (2006): 111–133.

96. F. Damiani, M. G. Giuliano, S. Cornuti, et al., "Multi-Site Investigation of Gut Microbiota in CDKL5 Deficiency Disorder Mouse Models: Targeting Dysbiosis to Improve Neurological Outcomes," *Cell Reports* 44 (2025): 115546.

97. M. A. Kayala and P. Baldi, "Cyber-T Web Server: Differential Analysis of High-Throughput Data," *Nucleic Acids Research* 40 (2012): W553–W559.

98. P. Baldi and A. D. Long, "A Bayesian Framework for the Analysis of Microarray Expression Data: Regularized t -Test and Statistical Inferences of Gene Changes," *Bioinformatics* 17 (2001): 509–519.

99. J. Folch, M. Lees, and G. H. Sloane Stanley, "A Simple Method for the Isolation and Purification of Total Lipides From Animal Tissues," *Journal of Biological Chemistry* 226 (1957): 497–509.

100. V. Totaro, L. Lupori, and T. Pizzorusso, *CounTastic: A MATLAB-Based Software for Cell Counting* (Zenodo, 2025), https://doi.org/10.5281/ZENODO.14761458.

101. L. Lupori, S. Cornuti, R. Mazziotti, et al., "The Gut Microbiota of Environmentally Enriched Mice Regulates Visual Cortical Plasticity," *Cell Reports* 38 (2022): 110212.

Supporting Information

Additional supporting information can be found online in the Supporting Information section. **Supplementary Table 1.** Statistical analysis of BW changes and OGTT, related to Figure 1. **Supplementary Table 2.** Hippocampus RNA-seq data, related to Figures 3 and S3. **Supplementary Table 3.** GO analysis of Hippocampus RNA-seq data, related to Figure 3. **Supplementary Table 4.** Liver RNA-seq data, related to Figures 4 and S4. **Supplementary Table 5.** GO analysis of Liver RNA-seq data, related to Figure 4. **Supplementary Table 6.** Statistical analysis of BW changes and OGTT, related to Figure 5. **Data S1:** Supplementary Figures 1–5.